



LAWRENCE
LIVERMORE
NATIONAL
LABORATORY

A Detailed Chemical Kinetic Reaction Mechanism for n-Alkane Hydrocarbons from n-Octane to n-Hexadecane

C. K. Westbrook, W. J. Pitz, O. Herbinet, E. J. Silke, H. J. Curran

September 25, 2007

Western States Section of The Combustion Institute
Livermore, CA, United States
October 16, 2007 through October 17, 2007

Disclaimer

This document was prepared as an account of work sponsored by an agency of the United States Government. Neither the United States Government nor the University of California nor any of their employees, makes any warranty, express or implied, or assumes any legal liability or responsibility for the accuracy, completeness, or usefulness of any information, apparatus, product, or process disclosed, or represents that its use would not infringe privately owned rights. Reference herein to any specific commercial product, process, or service by trade name, trademark, manufacturer, or otherwise, does not necessarily constitute or imply its endorsement, recommendation, or favoring by the United States Government or the University of California. The views and opinions of authors expressed herein do not necessarily state or reflect those of the United States Government or the University of California, and shall not be used for advertising or product endorsement purposes.

A Detailed Chemical Kinetic Reaction Mechanism
For n-Alkane Hydrocarbons
From n-Octane to n-Hexadecane

By

Charles K. Westbrook, William J. Pitz
Olivier Herbinet, Emma J. Silke, and Henry J. Curran*

Lawrence Livermore National Laboratory
Livermore, CA 94550 USA

*University College of Ireland
Galway, Ireland

Abstract

Detailed chemical kinetic reaction mechanisms have been developed to describe the pyrolysis and oxidation of the n-alkanes, including n-octane ($\text{n-C}_8\text{H}_{18}$), n-nonane ($\text{n-C}_9\text{H}_{20}$), n-decane ($\text{n-C}_{10}\text{H}_{22}$), n-undecane ($\text{n-C}_{11}\text{H}_{24}$), n-dodecane ($\text{n-C}_{12}\text{H}_{26}$), n-tridecane ($\text{n-C}_{13}\text{H}_{28}$), n-tetradecane ($\text{n-C}_{14}\text{H}_{30}$), n-pentadecane ($\text{n-C}_{15}\text{H}_{32}$), and n-hexadecane ($\text{n-C}_{16}\text{H}_{34}$). These mechanisms include both high temperature and low temperature reaction pathways. The mechanisms are based on previous mechanisms for n-heptane, using the same reaction class mechanism construction developed initially for n-heptane. Individual reaction class rules are as simple as possible in order to focus on the parallelism between all of the n-alkane fuels included in the mechanisms, and there is an intent to develop these mechanisms further in the future to incorporate greater levels of accuracy and predictive capability. Several of these areas for improvement are identified and explained in detail. These mechanisms are validated through comparisons between computed and experimental data from as many different sources as possible. In addition, numerical experiments are carried out to examine features of n-alkane combustion in which the detailed mechanisms can be used to compare processes in all of the n-alkane fuels. The mechanisms for all of these n-alkanes are presented as a single detailed mechanism, which can be edited to produce efficient mechanisms for any of the n-alkanes included, and the entire mechanism, with supporting thermochemical and transport data, together with an explanatory glossary explaining notations and structural details, will be available on our web page when the paper is accepted for publication.

INTRODUCTION

Practical fuels for transportation and other system fuels consist of complex mixtures of many types of hydrocarbon and related chemical species. Jet fuels, diesel fuel, gasoline and natural gas contain hundreds and often thousands of distinct chemical compounds. While not every chemical species contained in a practical fuel has been studied independently, these species can be collected into structural classes in order to understand the combustion properties and construct surrogate mixtures for those practical fuels. Recent studies have shown that it is productive to represent these practical fuels in terms of several basic structural classes of compounds, including n-alkanes, branched or iso-alkanes, aromatics, polycyclic alkanes, olefins, naphthenes, and oxygenated hydrocarbons for gasoline [1], diesel fuel [2], and jet fuel [3,4]. Straight-chain or n-alkanes species are important components in all of these practical transportation fuels.

The structure of a hydrocarbon fuel has a profound impact on the ignition properties of that fuel. Empirical correlations between species molecular structure and ignition properties have existed for many years [5], based on experimental studies, and in recent years, the role of fundamental kinetic properties of these hydrocarbon fuels on ignition rates have finally become clear [6-8]. Straight-chain hydrocarbons are more easily ignited under engine conditions than branched-chain hydrocarbons, and these ignition properties are commonly quantified in terms of octane number for spark-ignition engines, and cetane number for diesel engines. Ignition properties are also of central importance in homogeneous charge, compression ignition (HCCI) engines and other configurations of similar behavior that involve low temperature combustion (LTC).

The familiar octane and cetane scales are both defined in terms of reference fuels which provide the practical limits to ignition properties. For both scales, there is a fuel that defines easy or early ignition and another fuel that defines late or difficult ignition. The fuel that defines 0 octane number or easy ignition in spark-ignition engines is n-heptane, and the fuel that defines 100 cetane number or easy ignition in diesel engines is n-hexadecane, and in both cases, the fuel that is easily ignited is an n-alkane. The fuel that defines poor ignition for both scales is a highly branched hydrocarbon, iso-octane for gasoline and 2,2,4,4,6,8,8-heptamethyl nonane for diesel. It is clear that, in defining reference fuels for gasoline and diesel fuel, each fuel requires a component that is very ignitable and another that is much less ignitable. Since the fuel components in gasoline are primarily molecules with 5 - 10 carbon atoms, n-heptane and iso-octane provide convenient highly-reactive and low-reactive molecules. In diesel fuel, dominated by fuel components of higher molecular weights than gasoline, the highly ignitable component is n-hexadecane and the less ignitable component is heptamethyl nonane.

The easily ignited fuels, n-heptane and n-hexadecane, are noteworthy for the extensive amounts of low temperature, alkylperoxy radical isomerization, kinetic reactions that they produce, and this low temperature reactivity is an essential part of their rapid, early ignition kinetics. In general, n-alkanes exhibit considerable amounts of low temperature reactivity, which promotes early ignition. The highly branched fuels

that define the low-reactivity limits of the octane and cetane scales are slow to react because they exhibit little or no low temperature reactivity.

The present work focuses on the highly reactive n-alkane species that define the most ignitable limits of gasoline and diesel fuel. Since the practical reference fuels are n-heptane and n-hexadecane, the present work is intended to provide a computational model for all of the n-alkane fuels from n-heptane to n-hexadecane, building on the structural similarities between them to simplify the process of mechanism construction. This family of n-alkane fuels also makes it possible to study the effects of fuel molecule size on combustion properties, with all of the fuels having the same general molecular structure. In addition, n-alkanes have received a considerable amount of attention in experimental studies, although the large molecular size of many of these fuels and their correspondingly low vapor pressure have limited the number of experimental studies. For kinetic studies of n-alkanes as a family of molecules, intercomparisons of combustion properties demonstrate the importance of the length of the hydrocarbon chain, generally independent of other kinetic properties.

We have had some success modeling both laboratory-scale experiments and practical engine phenomena with our past n-heptane mechanism [9], and this paper reports on the results of extending the same methodology from C_7 to C_{16} n-alkanes. Most important, the work of Curran et al. [9,10] defined kinetic mechanisms for large hydrocarbons in terms of specific reaction classes and exploited a modular form for mechanism construction that we have again employed in the present work. This type of construction has been used frequently by others (e.g., [11-13]) and makes it quite simple to improve different reaction class descriptions as guided by new kinetics research.

The present reaction mechanisms are an attempt to provide “comprehensive” kinetic mechanisms, which are intended to use a wide variety of experimental inputs to validate the mechanisms [14,15]. In many cases, this means using experimental results from shock tube, flow reactor, rapid compression machine, static reactor, stirred reactor, laminar flame, opposed flow flame, engine, and any other types of experiments to test and validate the reaction mechanism. Comprehensive mechanisms for many fuels have been developed [9,10,16-23], largely for hydrocarbon molecules for which many types of experiments have addressed kinetic properties. Unfortunately, for the large n-alkanes of interest in this paper, there are relatively few such experimental studies that provide good validation results. The present work includes as many as possible of such validation data, but they are rather sparse and limited in range.

Comprehensive chemical kinetic reaction mechanisms, such as those reported here, are inherently always “works in progress” which are often updated and upgraded continuously, and this is certainly the case for these n-alkane fuels. As we will describe in greater detail below, we are aware of many specific details in each mechanism and other areas in which we plan to improve them. At the same time, the past success of the base n-heptane mechanism in many applications, as well as the overall good success of these new mechanisms at reproducing the limited variety of experimental results available, suggest that should be useful in their current form.

The present combined n-alkane model is new in the sense of simultaneously providing a powerful chemical kinetic tool for an important range of practical hydrocarbon fuels, all with the same structural type, from n-octane to n-hexadecane. However, an impressive variety of kinetic mechanisms have been developed by other authors for some of the fuels included in the present mechanism.

An early detailed kinetic mechanism was developed in 1992 for n-hexadecane by Chevalier et al. [24], which included both high and low temperature reaction pathways and was used to simulate engine knock phenomena. This mechanism was already quite large, with approximately 1200 species and 7000 elementary reactions, and it was generated by a LISP language that specified rules for rates of various reaction types.

The EXGAS code system developed at the DCPR/CNRS in Nancy [25-29] has been used to generate kinetic mechanisms for n-decane and n-hexadecane, and the group at Orleans has also developed kinetic mechanisms for n-decane and n-hexadecane [30-32]. Most of these mechanisms were tested through comparisons between model calculations and experimental results, primarily from the Orleans jet-stirred reactor (JSR), which were carried out within the high temperature regime, making it unnecessary at that time to include low temperature kinetic phenomena. The work of Dagaut et al. [32] used n-decane as surrogate to represent the kinetics of kerosene, and the same group have continued to develop continually more detailed kinetic models based on n-decane to represent the practical jet fuel kerosene. More recently, their work [33-34] has focused on using n-decane together with other surrogate compounds, especially cycloalkanes and aromatics, to better represent the soot production and emissions properties of kerosene. Dagaut et al. [35-36] recently extended this same approach to use a kinetic mechanism for n-hexadecane to simulate oxidation of rapeseed oil methyl ester. These important models have been very successful in their analyses of JSR oxidation of these large n-alkane fuels. Both kinetics groups have implemented low temperature reaction mechanisms in their kinetic models [25,37,38].

Nehse et al. [39] developed a detailed kinetic reaction mechanism for n-decane as well as an n-heptane and used these models to simulate intermediate shock tube experiments for both fuels. These mechanisms included both high and low temperature reaction mechanisms and were tested for a variety of experimental problems as discussed below. Olchanski and Burcat [40] developed a somewhat reduced high temperature kinetic mechanism for n-decane and used it to examine reflected shock wave ignition delay experiments that they had performed. Bikas and Peters [41] also developed a full temperature range kinetic mechanism to carry out an extensive series of n-decane combustion simulations in laminar flames, jet-stirred reactors, and shock tubes. Zhao et al. [42,43] developed a skeletal kinetic mechanism for n-decane oxidation that was limited to high and intermediate temperatures, which therefore was unable to address low temperature conditions. However, its most important contribution, due to its skeletal construction based on partial equilibrium among alkyl radicals as developed in earlier studies of n-heptane [44], lies in its ability to carry out highly efficient simulations under the experimental conditions for which it was intended to apply. Recent kinetic modeling

of pyrolysis in n-dodecane by Herbinet et al. [45] and Dahm et al. [46] have used the EXGAS approach to provide kinetic mechanisms to study pyrolysis of n-dodecane. Finally, Lindstedt and Maurice [47,48] followed their production of an important n-heptane mechanism with an extension to n-decane.

A number of reviews of n-alkane combustion have appeared recently, each of which surveys kinetic modeling approaches as well as the relevant literature of experimental studies that can be used for model validation. Dagaut and Cathonnet [49] summarized a large body of experiments and kinetic modeling of kerosene combustion, showing how n-decane kinetic models were first used to simulate kerosene oxidation, and the subsequent extensions of the modeling to enable the mechanisms to predict sooting behavior as well as overall heat release.

Buda et al. [50] discussed the values of developing unified kinetic mechanisms for alkanes over both the low and high temperature regimes, which is an approach very similar to that which has motivated the present paper. Similarly, Ranzi et al. [51] reviewed their “lumped” mechanism development approach which was then applied to provide mechanisms for n-decane, n-dodecane and n-hexadecane. With the Ranzi techniques, the mechanism lumping reduces the size of each mechanism and makes the resulting simulations reasonably efficient.

Finally, Battin-Leclerc [52] has carried out a very recent review of low temperature experiments and kinetic models, intercomparing the existing kinetic models for this regime. This work is an important resource for the present paper and will be extremely useful for future kinetic modeling.

In the current work, most of these past studies are used and built upon to construct and validate a family of chemical kinetic reaction mechanisms for large n-alkane fuels. The resulting kinetic mechanisms provide a useful set that researchers can use for a variety of applications, and we are making it available in modular form on our web page. Because of this modularity, it is quite simple to discard those portions that relate to n-alkanes larger than one which is targeted for study. Similarly, the set of mechanisms are ordered logically so that the submechanisms relevant to low-temperature problems can be eliminated to provide a smaller, high temperature mechanism for applications such as flame propagation and some classes of high temperature shock tube, flow reactor, and stirred reactor applications. The different n-alkanes are modeled using a self-consistent kinetic approach, so that the differences in their predictions are due only to the different sizes of the fuels, not to different submodels or assumptions made in parts of each mechanism. When future modifications are made to portions of any mechanism, the same modifications will be made simultaneously for all the n-alkanes, with the goal being to keep the kinetic approach as similar as possible from one n-alkane to all the others. These mechanisms are validated in this paper as thoroughly as possible, given that relatively few kinetic studies have been reported for many of these larger n-alkanes. In some cases, the same experiments are simulated for each of the $C_7 - C_{16}$ mechanisms, and this approach leads to some very interesting insights to hydrocarbon ignition that have not been previously appreciated.

KINETIC MECHANISMS

Basic Assumptions

Few kinetic studies have addressed site-specific reaction rates or product pathways for fuels with 8 or more carbon atoms, including those examined in the present study, so there are virtually no elementary reactions for which experimental rate expressions have been measured directly. In addition, chemical reaction rate theory becomes expensive in computational terms as the number of heavy atoms exceeds 5 or 6. As a result, it is necessary to employ rules of similarity for the rates and products of the very large number of reactions in these models. Those rules or other reasons for using specific reaction rates are described in the text below. In cases where transition-state theory [53,54] or other theoretical approaches can provide better rate expressions, it is straightforward to replace the present approximate expressions with improved versions. In addition, sensitivity analyses suggest that in many cases, the specific reaction rate expression for any given elementary reaction can be less important than the proper identification of its product distribution.

We have used the THERM software [55] to compute thermochemical data for the species involved in the C₈ – C₁₆ n-alkane kinetic mechanisms. This provides an internally consistent set of values for specific heats, heats of formation, enthalpies of formation and bond strengths that then produce consistent equilibrium constants and reverse reaction rates. There are other excellent alternative sources for thermochemical data (e.g., Yu et al. [56]) that could also be used, and the data computed using THERM may not be the best choices in some cases. The principle of the current work is that the modular mechanism construction and the clear way in which the thermochemical and kinetic data are presented should make it straightforward for anyone to exchange one set of thermochemistry for another as desired.

We use the reaction classes of Curran et al. [9,10] to present the details of the current mechanisms, and in many cases those reaction classes are retained intact. However, in a few cases, we find it desirable for increased clarity to subdivide a class to add new details that were not originally present in the Curran et al. prescriptions. In some other cases, we have used somewhat simpler and perhaps less accurate rate expressions than in the n-heptane and iso-octane mechanisms, again to provide simplicity and clarity.

Following our previous practice, we will provide all of the new reaction mechanisms on our Web page at:

http://www-cmls.llnl.gov/?url=science_and_technology-chemistry-combustion

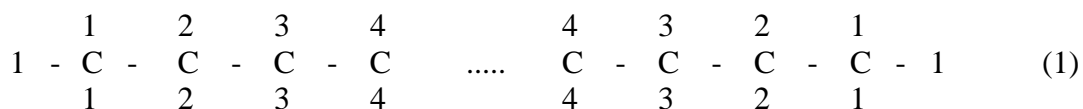
together with the required thermochemical tables and transport coefficients. They are presented in Chemkin-compatible format, based on the widespread usage of that format. Again, the modularity of the mechanism presentation should enable relatively simple

mechanism conversion to alternative formats. They are listed as one full mechanism, in a modular format to expedite editing to produce submechanisms as desired for specific n-alkanes smaller than C₁₆. In addition to simplified elimination of families of species and reactions larger than required for particular applications, the present format also makes it straightforward to remove species and reactions intended only for low-temperature oxidation applications

We intend to refine and improve the present mechanisms in a number of ways in the near future. Among the major upgrades anticipated are (1) a more general treatment of O₂QOOH isomerization reactions to include alternative reaction pathways, (2) implementation of the direct molecular elimination reaction path for production of olefin + HO₂ from decomposition reactions of certain alkylperoxy radicals, (3) three-parameter reaction rate expressions for addition reactions of alkyl + O₂ and QOOH + O₂ reactions, and (4) increased detail in reaction submechanisms for oxidation of large olefin species, including site-specific H atom abstraction reactions and retroene decomposition reactions. Those and other expected changes are described in detail within the discussions of the specific reaction classes below. The web-based mechanism files will be updated as these major mechanism improvements are made, along with documentation of the upgrades, although the earlier versions will also continue to be available. However, those changes are intended to improve the theoretical underpinnings for the mechanisms, and they are not required for many productive uses of the current mechanisms, as illustrated by the validation studies included below. We anticipate applying the same types of mechanism upgrades to previously existing mechanisms for n-heptane and other heptane isomers, as well as isomers of hexane and pentane.

Notation

The specific details of the notation are summarized online as part of the mechanism documentation, but the simplest terms are described here for completeness. For a given n-alkane, we number the C atoms from one end of the linear chain, employing the reflection symmetry of this type of chain. Therefore, we can write:



showing the first 4 C atoms at the ends of an n-alkane chain. The numbers in Eq. (1) indicate H atoms in this n-alkane as well as the numbering of the H atom sites corresponding to the number of the C atom to which they are bonded. We number the C atoms as shown as the '1' site, the '2' site and continuing to the midpoint of the chain, then using the reflection symmetry to also number the sites from the opposite end of the

chain. For n-hexadecane, the two middle C atoms would have the index '8'; for n-pentadecane there is only one '8' carbon atom, while for n-tetradecane there are two '7' C atoms and for n-tridecane there is only one '7' C atom. In the mechanisms, n-alkanes are named 'nc10h22' for n-dodecane, and similarly for the other n-alkanes.

There are therefore 3 H atoms attached at primary bonding sites at each end of these n-alkanes and indicated as '1' H atoms, with a total of 6 '1' H atoms in each n-alkane molecule. All of the other H atoms are bonded at secondary sites. The unique numbering of these secondary H atoms is intended to show that all of the '2' H atoms (of which there are four in the above diagram) are structurally identical and different from all the other sites, all of the '3' sites are also structurally identical and unique from all the other sites, and similarly for the remaining H atoms. The uniqueness of each of these sites leads to unique reaction product distributions to H atom abstraction and subsequent reactions. This is a key feature of a truly detailed, as opposed to a lumped or reduced reaction mechanism. These distinctions add a great deal to the complexity and size of a detailed reaction mechanism, but they also provide greater detail that may or may not justify the additional complexity, depending on the level of detail required. This type of detailed mechanism can subsequently be reduced by lumping together selected families of structurally similar species with overall reaction rates, and the existence of the more fully detailed mechanism can then be very helpful in testing the capabilities of the reduced mechanism.

Alkyl radicals are indicated based on the H atom that has been removed from the chain above. Thus the c9h19-3 species indicates the result of abstracting a '3' H atom from n-nonane, while c16h33-7 represents the alkyl radical produced by abstracting a '7' H atom from n-c16h34. Subsequent addition of molecular oxygen to the c9h19-3 alkyl radical is shown by 'c9h19o2-3', the related alkoxy radical is 'c9h19o-3' and the related hydroperoxide is 'c9h19o2h-3'. We expect to provide a full glossary of these and other mechanism notation details on the mechanism web site.

Reaction Classes

Each of these classes have been discussed in some detail in the mechanism descriptions for n-heptane [9] and iso-octane [10]. It should be noted that the "rules" for each of the reaction classes were not all the same in these two past studies, reflecting 4 years of mechanism development between the two mechanisms. For the current n-alkane mechanisms, we have chosen in some cases to return to the reaction class rules used for n-heptane, which are somewhat less refined than those for iso-octane. However, the initial purpose of the present study of larger n-alkanes was to provide the most transparent and obviously parallel possible set of reaction rate rules, and in some cases this parallelism was obscured in the iso-octane mechanism of reference [10]. As noted above, this initial, somewhat simplified mechanism is in a convenient modular form for future upgrades as they become available, and those improvements can be made simultaneously for all of the n-alkane fuels.

In the discussion below, we will identify the improvements that are planned for some of these reaction classes. Battin-Leclerc [52] has presented an excellent analysis of many of the same issues, and our future development will benefit from that work. However, many of these mechanism refinements are not expected to modify the most important features of the model predictions except as noted below.

An overall reaction path diagram for hydrocarbon combustion in general and ignition in particular is shown in Figure 1.

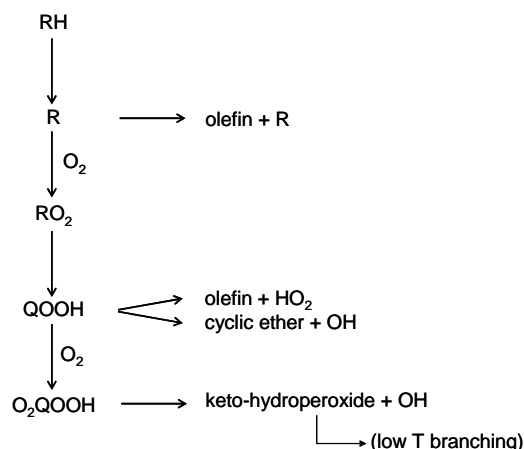


Fig. 1. Overall reaction path diagram describing hydrocarbon ignition at high and low temperatures.

Reaction Class 1: Unimolecular fuel decomposition

These reactions produce two alkyl radicals or one alkyl radical and one H atom. They provide chain initiation and, as the size of the hydrocarbon fuel increases, significant fuel consumption as well. Due to very high activation energies, the reactions producing H atoms are usually important only in the recombination direction, where they serve as sinks for H atoms. We prescribe the reaction rates in the exothermic or recombination direction, using the same rules and temperature-independent rates as in our previous n-heptane mechanism [9], and the rates in the decomposition direction are determined from microscopic reversibility and the thermochemistry of the individual species. For alkyl+H reactions, we assume a rate of $1 \times 10^{14} \text{ cm}^3 \text{ mol}^{-1} \text{ s}^{-1}$; when the recombination reactants include a methyl radical, we use a rate of $1 \times 10^{13} \text{ cm}^3 \text{ mol}^{-1} \text{ s}^{-1}$, and when both recombination reactants are larger alkyl radicals, we assume a rate of $8 \times 10^{12} \text{ cm}^3 \text{ mol}^{-1} \text{ s}^{-1}$.

Reaction Class 2: H-atom abstractions

These reaction rates depend on the abstracting radical, on the type of C - H bond that is being broken, which for these fuels are primary and secondary C - H bonds, and on the number of H atoms at equivalent sites. These values are similar to, but not identical to

those in our past mechanisms [9,10]. There are no tertiary C - H bonds in any of the n-alkane fuels discussed in the present work.

Reaction Class 3: Alkyl radical decomposition

Alkyl radical decomposition is important at temperatures above about 850K; below this temperature, alkyl radical addition to molecular oxygen is the major pathway for alkyl radical consumption. Because alkyl radical decomposition via β -scission is endothermic, we calculate the rate constant in the reverse, exothermic direction that is the addition of an alkyl radical (or H atom) across the double bond of an alkene, then computing the forward, β -scission rate constant to calculated from thermochemistry.

Reaction rate expressions for the reactions are very similar to those used in past reaction mechanisms for n-heptane and iso-octane. Rate constants for the addition of radicals across a double bond depend on (1) the site of addition (i.e., a terminal or internal C atom), and (2) the type of radical being added. Based on the work of Allara and Shaw [57], we assume that addition of an H atom across a double bond has a pre-exponential A-factor of $1 \times 10^{13} \text{ cm}^3 \text{ mol}^{-1} \text{ s}^{-1}$ with an activation energy of 1200 cal/mol if the H atom adds to the terminal C atom of the alkene, and with 2900 cal/mol if the H atom adds to an internal C atom. The rate constant for the addition of an alkyl radical has a lower A-factor and higher activation energy than for the addition of an H atom. We assume an A-factor of $1 \times 10^{11} \text{ cm}^3 \text{ mol}^{-1} \text{ s}^{-1}$ and an activation energy of 8200 cal/mol. We assume all these reactions are at their high pressure limit for the conditions of this study.

Reaction Class 4: Alkyl radical + O₂ = olefin + HO₂

This reaction class was discussed at some length in our paper on n-heptane [9], with a number of reasons why this direct reaction pathway was not included in our earlier reaction mechanism. During the intervening years, a number of very interesting studies [58-61] of these reactions have led to the conclusion that a direct, molecular elimination reaction of RO₂ can produce an olefin + HO₂ without proceeding via a QOOH intermediate and should be included in low temperature kinetic mechanisms. Most of the relevant research has focused on small hydrocarbon species such as ethyl and propyl radicals, and it is not yet clear if the same reactions occur for radicals as large as those in the present mechanisms, or what the rates of those reactions might be. This reaction type will be examined for these mechanisms in the future. However, the present mechanisms, without this direct reaction, include sufficient detail in the reaction pathways available to the large alkyl radicals to describe n-alkane oxidation adequately.

Our recent kinetic modeling studies, including n-heptane [9], cyclohexane [62] and methyl cyclohexane [63], have shown that the key to reproducing the overall rate of oxidation and the correct amount of NTC behavior is an accurate description of the relative rates of chain branching, chain propagation, and chain termination in the reactions of the alkyl radicals from the fuel. The direct decomposition reaction of alkylperoxy radicals, producing an olefin and HO₂, is a propagation reaction pathway, so

if this reaction class is added to the overall n-alkane mechanisms, then one or more corresponding changes will be needed to restore the proper balance of propagation with branching reaction paths. Either existing propagation reaction rates involving alkyl radicals must be reduced to compensate for the propagation provided by including the direct molecular elimination reaction, or the rates of chain branching pathways would have to be increased correspondingly. This process was in fact already implemented successfully in the case of cyclohexane oxidation [62]. However, the present treatment is suitable for most applications for the time being.

Reaction Class 5: Alkyl radical isomerization

These reactions transfer H atoms from one site in the radical to another via internal abstraction steps. Reaction rates depend on the type (i.e., primary, secondary or tertiary) of C - H bond being broken, on the ring strain energy of the transition state ring involved, and on the number of equivalent H atoms available. The overall activation energy E_a is estimated using the expression

$$E_a = \Delta H_{\text{rxn}} + \text{ring strain} + E_{\text{abst}}$$

where ΔH_{rxn} is the enthalpy of reaction if the reaction is endothermic and zero otherwise. The activation energy for reaction is determined [64] from an Evans-Polanyi plot of E_{abst} vs ΔH_{rxn} (taken in the exothermic direction) of similar H atom abstraction reactions, leading to the following expression:

$$E_{\text{abst}} = 12.7 + (\Delta H_{\text{rxn}} \times 0.37)$$

The A factors were obtained using RADICALC [65], a computer code that implements transition state theory and calculates the change in entropy of the radical to the transition state due to loss or gain of internal rotors and optical isomers.

At temperatures close to 1000K, these processes are quite rapid, creating an effective equilibrium among all the alkyl radicals. The rates of alkyl β -scission have higher activation energies than the energy barriers for isomerization, so under such conditions the decomposition of alkyl radicals takes place from an equilibrium pool of alkyl radicals. Dryer et al. [42-44] have exploited this feature in the reaction mechanisms of a number of complex fuels to reduce the mechanisms significantly for more efficient computations, at little or no loss of generality. However, this process can be done only for a range of temperatures around 1000K where isomerization is rapid and β -scission is slow.

Reaction Class 6: H atom abstraction from olefins

Very few detailed kinetic mechanisms are available for any large olefin species, including those included in the present n-alkane mechanisms. Battin-Leclerc [52] has surveyed the entire literature and found no olefins larger than pentene with kinetic reaction mechanisms that distinguish between olefin isomers and provide site-specific reaction rates for elementary reactions. New work, not yet published, by Mehl et al. [66] has developed a kinetic mechanism for the isomers of hexene and used that mechanism to study RCM experiments of Vanhove et al. [67], but overall this is an area in which a great deal more kinetic research is needed.

In order to oxidize the olefins produced in the present n-alkane mechanisms, we have estimated rates for H atom abstraction reactions from the olefin species. Abstracting radicals are limited to H, OH, O, and CH₃ radicals and the products are lumped into a single alkenyl radicals for each n-alkane fuel. Thus there is only one C₁₀H₁₉ radical in the n-decane mechanism, and only one C₁₆H₃₁ alkenyl radical in the n-hexadecane mechanism. This is a serious over-simplification and more work is needed. If the fuel consists of an n-alkane fuel, sensitivity analyses have indicated that the present simplified treatment of the alkenyl radicals is satisfactory, but when the fuel is a large n-olefin, this simplification is not likely to be suitable.

Reaction Class 7: Addition of radical species to olefins

This reaction type is treated in the same manner as in past mechanisms for n-heptane and iso-octane. Addition of H atoms and CH₃ radicals are already included as the reverse direction of β -scission reactions in Reaction Class 3. Addition of HO₂ radicals are also included as described below for Reaction Class 20. The remaining radical additions of O and OH are treated as a composite reaction. In principle, these reactions involve addition of the O or OH radical to one or the other side of the olefin double bond. In our treatment, the resulting oxygenated adduct is not treated as a separate species but is assumed to decompose via a β -scission type of reaction. In the present mechanisms, we have attempted to identify the most likely product distributions for these decompositions and include the overall reaction as an “elementary” reaction. Like several other features of these n-alkane reaction mechanisms, this approach is satisfactory when the primary fuel under examination is an alkane, but when the primary fuel is an olefin, this treatment should be refined further to include a more detailed description.

Reaction Class 8: Alkenyl radical decomposition

The present n-alkane mechanisms include a somewhat improved treatment of the decomposition of the lumped alkenyl radicals, as compared with the prior treatment of our n-heptane and iso-octane mechanisms [9,10]. While there is only a single alkenyl radical for each n-alkane fuel, the alkenyl radical is now assumed to decompose to a wide range of smaller products, with each decomposition reaction producing a smaller olefin and a smaller alkenyl species. In the absence of a much more careful kinetic modeling of

n-olefins and their products, this lumping of alkenyl radicals and the detailed variety of their decomposition reactions is a temporary but effective solution. All of the decomposition reactions are assigned a rate expression of $1.0 \times 10^{13} \exp(-45000/RT) \text{ s}^{-1}$.

Reaction Class 9: Olefin decomposition

In model computations, large olefin species decompose at appreciable rates. For all of the present mechanisms, we have used the same rate constant expression of $1 \times 10^{16} \exp(-71000/RT) \text{ s}^{-1}$. In previous large molecule mechanisms, we used an A-factor of 2.5×10^{16} , but in the present mechanisms, we have included a larger variety of product pathways for each olefin and reduced each A-factor to give approximately the same overall rate of olefin decomposition. This is a very simplified treatment of a complex set of reactions, and more research is needed to refine this subject area.

LOW TEMPERATURE MECHANISM

The following reaction classes are frequently identified as “low temperature” reaction pathways, which is somewhat oversimplified. First, the transition from high to low temperature regimes is not sharply defined, and increasing pressure can extend the “low temperature” regime to higher temperatures. The key overall is Reaction Class 10, the addition of molecular oxygen to alkyl radicals and the equilibrium constant of such addition reactions. If this equilibrium strongly prefers the adduct RO_2 , then the “low temperature” reaction sequences will contribute to the rate of combustion, and if the equilibrium strongly favors the dissociation to $\text{R} + \text{O}_2$, then only the Reaction Classes 1 - 9 are generally required. Much of the low temperature kinetic mechanism is based on the work of Pollard [68].

Reaction Class 10: Alkyl radical addition to O_2

Rates of addition reactions of radical species to O_2 were assumed to depend on the type (primary, secondary, or tertiary) of alkyl radical to which the O_2 is added. For the present mechanisms, we have selected a single addition rate and decomposition rate for each of the two types of alkyl radicals in these n-alkane fuels. These rates are approximately correct, and there are many studies on which to base subsequent refinements. For the present, the simplified treatment will provide a good basis for mechanism comparisons, and future improvements will provide better descriptions of variations of the equilibrium of these reactions with temperature and pressure.

In the present mechanisms, for primary alkyl radicals, the $\text{R} + \text{O}_2$ addition reactions all have the same rate expression of $4.52 \times 10^{12} \text{ cm}^3 \text{ mol}^{-1} \text{ s}^{-1}$ and decomposition rate expressions of $2.66 \times 10^{20} \text{ T}^{-1.67} \exp(-35400/\text{RT}) \text{ s}^{-1}$. For secondary alkyl radicals, all of the addition reactions have the rate expression of $7.54 \times 10^{12} \text{ cm}^3 \text{ mol}^{-1} \text{ s}^{-1}$ and decomposition rate expression of $1.36 \times 10^{23} \text{ T}^{-2.36} \exp(-37670/\text{RT}) \text{ s}^{-1}$.

Reaction Class 11: $\text{R} + \text{R}'\text{O}_2 = \text{RO} + \text{R}'\text{O}$

Reactions of alkyl radicals with alkylperoxy radicals are estimated to occur at $7.0 \times 10^{12} \exp(+1000/\text{RT}) \text{ cm}^3 \text{ mol}^{-1} \text{ s}^{-1}$, as assumed in our previous iso-octane mechanism and close to the rate used in our n-heptane mechanism. The reverse rates are based on microscopic reversibility. We include only those reactions in which the R and R' alkyl radicals have the same number of carbon atoms. That is, for the n-dodecane mechanism, we include such reactions as $\text{C}_{12}\text{H}_{25}\text{-2} + \text{C}_{12}\text{H}_{25}\text{O}_2\text{-5} = \text{C}_{12}\text{H}_{25}\text{O-2} + \text{C}_{12}\text{H}_{25}\text{O-5}$, but we do not include $\text{C}_{12}\text{H}_{25}\text{-2} + \text{C}_{11}\text{H}_{23}\text{O}_2\text{-5} = \text{C}_{12}\text{H}_{25}\text{O-2} + \text{C}_{11}\text{H}_{23}\text{O-5}$. The reasoning for this choice is that we expect the R and $\text{R}'\text{O}_2$ levels to be significant only for the R and $\text{R}'\text{O}_2$ corresponding to the carbon number of the initial fuel, with the rates of all “cross

reactions” with R and R’ with different numbers of carbon atoms being negligibly slow because either the R or R’ would be orders of magnitude smaller than the other. We also include reactions of the form $R + HO_2 = RO + OH$, using the same rate expression of $7.0 \times 10^{12} \exp(+1000/RT) \text{ cm}^3 \text{ mol}^{-1} \text{ s}^{-1}$, used above. This group of reactions had not been included in either the n-heptane or iso-octane mechanisms and were included here for completeness.

Reaction Class 12: Alkylperoxy radical isomerization

These reactions provide the key reactions for low temperature hydrocarbon oxidation pathways. There is an extended discussion of the sources of these reaction rates in our iso-octane paper [10], and the individual rate expressions used for these n-alkanes are the same as those in reference [10]. The role of these reactions is to determine how much chain propagation and how much chain branching occurs within the low temperature oxidation regime. The transition state rings which are included in this Reaction Class have 5, 6, 7, and 8 atoms, and the elementary rates vary with the size of the transition state ring (i.e., ring-strain energy barrier), and the type of C - H bond that is broken to transfer the H atom. The importance of these reactions is that, to a large extent, the 5-membered transition state rings produce chain propagation, the 6-membered transition state rings produce chain branching, and the 7- and 8-membered transition state rings also produce chain propagation. The product distributions of low temperature oxidation also are different for each transition state ring size, and this information is needed to calibrate all of the reaction rate parameters for this class of reactions.

Reaction Class 13: $RO_2 + HO_2 = ROOH + O_2$

This reaction class uses a rate expression of $1.75 \times 10^{10} \exp(+3275/RT) \text{ cm}^3 \text{ mol}^{-1} \text{ s}^{-1}$, the same as in our previous iso-octane mechanism and similar to that in the n-heptane mechanism. The reverse reaction rate is computed using microscopic reversibility. This reaction is relatively unimportant because other reactions of RO_2 are usually much faster than this bimolecular reaction.

Reaction Class 14: $RO_2 + H_2O_2 = ROOH + HO_2$

This reaction rate expression is the same as that for previous mechanisms, $2.4 \times 10^{12} \exp(-10000/RT) \text{ cm}^3 \text{ mol}^{-1} \text{ s}^{-1}$, based on Tsang’s recommendation [69] for the reaction $CH_3O_2 + H_2O_2 = CH_3O_2H + HO_2$. This reaction is isoergic, and the reverse reaction has the same rate as the forward reactions.

Reaction Class 15: $\text{RO}_2 + \text{CH}_3\text{O}_2 = \text{RO} + \text{CH}_3\text{O} + \text{O}_2$

The only reaction of this type that has been studied in detail is $\text{CH}_3\text{O}_2 + \text{CH}_3\text{O}_2 = \text{CH}_3\text{O} + \text{CH}_3\text{O} + \text{O}_2$. We estimated the rate of this reaction is our iso-octane mechanism to be $1.40 \times 10^{16} \text{ T}^{-1.61} \exp(-1860/\text{RT}) \text{ cm}^3 \text{ mol}^{-1} \text{ s}^{-1}$, and this rate expression is used in the present mechanisms. We assume that the termolecular reverse reaction has a zero rate.

Reaction Class 16: $\text{RO}_2 + \text{R}'\text{O}_2 = \text{RO} + \text{R}'\text{O} + \text{O}_2$

The rate expressions for this class are assumed to be the same as those above for Class 15, which was also done in the iso-octane mechanism. As in Class 11, we assume the rates of these reactions are significant only when $\text{R} = \text{R}'$, that is, when both R and R' have the same number of carbon atoms.

Reaction Class 17: $\text{RO}_2\text{H} = \text{RO} + \text{OH}$

In early combustion kinetics analyses, this reaction was believed to be extremely important, following the abstraction of H atoms from the fuel and other stable hydrocarbons by RO_2 radicals. At lower temperatures, the decomposition of RO_2H would provide degenerate branching and contribute significantly to the onset of ignition. In more recent years, the greater importance of RO_2 isomerization reaction pathways has become recognized, and current kinetic modeling produces relatively minor levels of RO_2H . Decomposition of RO_2H can still be very important in situations where it is added to sensitize a reactive mixture, as some cetane improvers.

In the present mechanisms, we use a rate expression $1.5 \times 10^{16} \exp(-42500/\text{RT}) \text{ cm}^3 \text{ mol}^{-1} \text{ s}^{-1}$ when R is a primary radical and $1.25 \times 10^{16} \exp(-41600/\text{RT}) \text{ cm}^3 \text{ mol}^{-1} \text{ s}^{-1}$ when R is a secondary radical, reflecting the slightly different bond strengths of the O-O bonds, and similar to recommendations of Sahetchian et al. [70] for 1-heptyl and 2-heptyl hydroperoxides. The rate of the reverse reaction, in the recombination direction, is determined using microscopic reversibility.

Reaction Class 18: Alkoxy radical decomposition

These decomposition reactions are assumed to proceed via formation of an aldehyde and an alkyl radical, an analogy with β -scission reactions of large alkyl radicals. Like β -scission reactions, these reactions are written in the addition direction, with rate expressions of $1.0 \times 10^{11} \exp(-11900/\text{RT}) \text{ cm}^3 \text{ mol}^{-1} \text{ s}^{-1}$ when R is a primary radical and $1.0 \times 10^{11} \exp(-12900/\text{RT}) \text{ cm}^3 \text{ mol}^{-1} \text{ s}^{-1}$ when R is a secondary radical.

Reaction Class 19: QOOH decomposition and production of cyclic ethers

These reactions involve breaking the O-O bond in the QOOH radical, followed by the formation of a cyclic compound. The rates of these reactions are assumed to depend primarily on the number of atoms in the cyclic portion of the molecule, or equivalently, to the ring strain energy barrier to forming the cyclic structure. The major research issue regarding these reaction rates is the way the A-factors are estimated. As the size of the transition state ring grows, there is a loss of entropy as internal rotors are eliminated, and the A factor of the reaction decreases. In the n-heptane mechanism [9], the A-factors decrease by factors of 12 with each increase in the number of atoms in the transition state ring, but this factor of 12 was changed to a factor of 8 for the iso-octane mechanism [10] to better match the distributions of the product cyclic ethers, and these factors of 8 are retained in the present mechanism.

Reaction Class 20: QOOH beta decomposition to produce olefin + HO₂

When the radical site in the QOOH radical is on the C atom adjacent to the COOH group, the radical can decompose to produce an alkene and HO₂. The rates of all of these reactions are assumed to be the same, at $1.61 \times 10^{20} T^{-2.52} \exp(-21350/RT) \text{ s}^{-1}$ in the decomposition direction and $1.0 \times 10^{11} \exp(-11530/RT) \text{ cm}^3 \text{ mol}^{-1} \text{ s}^{-1}$ in the addition direction.

This reaction plays a significant role in determining the rate of low temperature ignition of hydrocarbons and the extent of NTC behavior. It represents a chain propagation route for RO₂ isomerizations, which compete with alternative reaction pathways that lead to chain branching. The balance between chain propagation and branching has been shown [62,63] to be the most important factor in reproducing the extent of NTC behavior. Recent studies [58-61] have indicated that a direct reaction of RO₂ proceeds through a direct molecular elimination path to produce a conjugate olefin and HO₂, rather than via QOOH intermediates; such direct eliminations pathways provide additional chain propagation, which therefore requires either reduced propagation via alternatives such as QOOH = olefin + HO₂ or increased chain branching in other reactions, in order to maintain the balance needed to reproduce observed NTC behavior. Experimental evidence [71] suggests that this QOOH = olefin + HO₂ reaction may have a somewhat higher energy barrier than is used in the present mechanism, and recent modeling results for low temperature oxidation of cyclohexane [62] demonstrated that a direct molecular elimination pathway for R + O₂ can be combined with a reduced rate of QOOH = olefin + HO₂ to retain the observed NTC behavior by maintaining the ratio of propagation to branching. We expect to revisit all of the RO₂ reaction pathways as the present mechanisms are upgraded in the future. However, the current mechanisms do provide the proper balance between propagation and branching and can reproduce observed behavior in hydrocarbon ignition at low temperatures.

Reaction Class 21: QOOH decomposition to small olefin, aldehyde and OH

When the QOOH radical is produced from RO₂ via a six-membered transition state ring, the QOOH can then decompose via a β-scission reaction to produce a carbonyl product and an olefin, followed by an O-O bond scission that produces OH; the overall products thus consist of OH, an aldehyde and an olefin. In our previous n-heptane mechanism, we assigned these reactions a direct decomposition rate expression, but in the iso-octane mechanism we assumed a rate expression for the addition of the olefin and the carbonyl species of $1.0 \times 10^{11} \exp(-11900/RT) \text{ cm}^3 \text{ mol}^{-1} \text{ s}^{-1}$ and then compute the β-scission reaction from this expression and microscopic reversibility. We characterize this process in the mechanisms as an “elementary” reaction with three products and a zero reverse rate, since we discount the possibility of the olefin, aldehyde and OH recombining to produce the QOOH original species. Since the olefin and aldehyde are relatively stable products, this reaction class is effectively a chain propagation pathway since it produces only one OH radical species.

Reaction Class 22: Addition of QOOH to molecular oxygen O₂

The addition reactions of QOOH with O₂ provide the only pathways at low temperatures that provide significant chain branching via production of multiple radical distributions, as outlined below. The equilibria of these reactions are strongly temperature dependent, with decomposition reaction activation energies of about 36 kcal/mol and addition reaction activation energies of approximately zero, and these equilibria are ultimately responsible for NTC behavior in the oxidation of these n-alkanes.

We have assumed that the rates of these addition reactions are the same as the addition reactions of alkyl radicals with O₂ described above for reaction class 10, varying only from the type (i.e., primary or secondary) of site in the QOOH species at which the addition occurs. In principle, the dissociation reaction rate expression is computed from the forward rate via microscopic reversibility. However, in the present mechanism, we have set all of the dissociation reactions involving reactions at primary sites equal to a single, characteristic dissociation rate expression, and another representative rate expression for dissociation involving secondary sites. We consider that any systematic inaccuracies in this process are less than the uncertainties in forward reaction rate expressions and the relevant equilibrium coefficients, but we expect to determine more specific dissociation reaction rate expressions in the future.

Reaction Class 23: O₂QOOH isomerization to carbonylhydroperoxide + OH

These reactions are quite complex, including an internal H atom abstraction via a cyclic transition state, followed by O-O bond breaking and then formation of a C=O carbonyl bond. The rate expressions for this class of reaction are the same as those for comparable RO₂ isomerization reactions in reaction class 12, except that the activation energies are reduced by 3 kcal/mol. This reduction is due to the fact that the H atom being abstracted

is bound to a carbon atom with a hydroperoxy group, which lowers the C-H bond energy by approximately 3 kcal/mol. In addition, the A-factors from O₂QOOH isomerization reactions must be adjusted to reflect the lower number of H atoms available at the target site due to the presence of the OOH group that has displaced one H atom site.

This current treatment assumes that the internal H atom transfer process is limited to H atoms at sites in the O₂QOOH species where the original H atom abstraction occurred in the n-alkane molecule. The reasoning, noted just above, is that the OOH group at the site of the initial H atom abstraction makes the remaining H atoms easier to abstract and that they will be the predominant pathway for isomerizations. However, many of the remaining H atoms at other sites in the O₂QOOH species can also be abstracted in isomerization steps, some of which can be more rapid than those included in the present formulation. We have included some of these “alternative” isomerization reaction pathways in previous mechanisms, particularly when the fuels are highly branched as in some isomers of heptane [7] or in fuels with limited numbers of conventional isomerization pathways [62], but they are not yet included in the present n-alkane mechanisms. In the case of n-alkanes, there are so many possible O₂QOOH isomerization pathways with relatively low activation energies that the inclusion of alternative pathways does not affect the rate of ignition to any significant degree, but future revisions of these mechanisms will add these reaction pathways.

Reaction Class 24: Carbonylhydroperoxide decomposition

Decomposition of these complex carbonylhydroperoxide species starts with breaking the O-O bond, followed by a series of radical decomposition steps that produces a carbonyl radical and a stable product, usually an aldehyde. Thus this reaction produces two radicals in addition to an aldehyde, which is a fairly reactive type of stable species, and the overall effect in the reaction mechanism is a considerable degree of chain branching. This reaction and its radical products complete the conditions necessary for ignition at low temperatures. As temperature increases, several kinetic processes adjust and eventually disconnect the necessary conditions, ending the ignition. The equilibrium of the R + O₂ and QOOH + O₂ reactions move towards becoming dissociation reactions, and the propagation reactions of QOOH steadily increase at the expense of the QOOH reactions that lead to chain branching. The region where these processes adjust is exactly the temperature range that we characterize as the NTC region.

We write this series of processes as a single reaction in the mechanism, in spite of the complexity of the multiple processes actually occurring. The rate for the “reaction” is estimated by recognizing that the first step involves breaking the O-O bond. Although the thermochemistry of each carbonylhydroperoxide species is different, we have assigned two rates for all of the possible decomposition reactions, one at $1.5 \times 10^{16} \exp(-42000/RT) \text{ s}^{-1}$ for all of the decompositions where the OOH is located at a primary C site and $1.05 \times 10^{16} \exp(-41600/RT) \text{ s}^{-1}$ for all of the decompositions where the OOH is located at a secondary C site, again based on recommendations of Sahetchian et al. [70] for decompositions of 1-heptyl and 2-heptyl hydroperoxides.

Reaction Class 25: Reactions of cyclic ethers with OH and HO₂

Cyclic ethers are produced at lower temperatures and consist of large hydrocarbons with oxygen atoms imbedded in the molecule. There is very little kinetic information, especially including site-specific reaction rates, that is available for this class of species. A cyclic ether produced from n-tetradecane would have the formula C₁₄H₂₈O with a cyclic ring of 3, 4, 5, or 6 atoms, one of which is the O atom in the molecule. Thus there is also a chain of carbon and hydrogen atoms of considerable length, and there is a good probability that H atom abstraction would be the major component of their consumption. Since these species are formed predominantly at low temperature, we have assumed that the most important H atom abstractions are those by OH and HO₂ radicals, which are the most significant radicals at lower temperatures. Abstraction reactions with H, O, CH₃ and other radicals can easily be included in a mechanism, especially if the large cyclic ethers were the primary fuels in a system, but as relatively minor species produced only at lower temperatures, the inclusion of abstractions only by OH and HO₂ seems justified. Also, since cyclic ethers from the large n-alkanes are produced only at low temperatures, reactions involving breaking C - C bonds are very unlikely to be significant consumers of the cyclic ethers. Again, if these species were parts of the primary fuel and present in significant amounts, then additional consumption pathways should be included.

Because these species are present only as minor intermediates, in the past we did not include site-specific reactions in the mechanism. Instead, we considered only averaged processes over all of the possible processes for H atom abstraction. The present mechanisms employ an averaging system that considers a wide range of H atom abstractions from the cyclic ethers. For each possible abstraction site, an estimated product distribution is assumed. Further development of this portion of these mechanisms would require extended study of oxidation of cyclic ethers as primary fuels, while for n-alkane fuels, this level of mechanism sophistication is probably appropriate.

The above detailed reaction mechanisms are built upon a core mechanism for the smaller C/H/O species. This is also done in most other large molecule mechanisms by others, where this core mechanism describes the H_2/O_2 and $\text{CO}/\text{H}_2/\text{O}_2$ reactions and usually $\text{C}_1 - \text{C}_4$ or $\text{C}_1 - \text{C}_5$ hydrocarbons. The core $\text{C}_1 - \text{C}_4$ submechanism for the present work has been developed by Curran [72] and is itself a constantly-evolving mechanism. It is included in the overall mechanism shown in our web page. As it is systematically improved, new versions will be inserted and the result again provided on our web page with its documentation, again preserving earlier versions.

These are large reaction mechanisms which require significant amounts of computer disk space and memory to execute. The mechanism for n-hexadecane includes 8130 elementary reversible reactions among 2116 chemical species, and these totals increase when additional submechanisms are added, such as a reasonably complete NOx submode or a soot submodel. Since we have written one combined mechanism in modular form for all of the n-alkanes up to n-hexadecane, it is simple to eliminate unnecessary submechanisms larger than needed for a specific application. This can reduce the size of the mechanism significantly.

The sizes of some of the fuel mechanisms from C_{10} through C_{16} when species and reactions for larger fuels have been removed are the following:

	$\text{C}_{16}\text{H}_{34}$	$\text{C}_{14}\text{H}_{30}$	$\text{C}_{12}\text{H}_{26}$	$\text{C}_{10}\text{H}_{22}$
Reactions	8130	6449	5030	3878
Species	2116	1668	1282	940

We have found that the $\text{C}_{12}\text{H}_{26}$ mechanism is the largest that can be used on the latest version of the latest version of the Chemkin code for a homogeneous, single zone problem such as a shock tube or stirred reactor, on a 32-bit computer such as a recent model laptop computer.

VALIDATION STUDIES

Unlike many smaller hydrocarbon fuels such as methane, propane or even n-heptane, the larger n-alkanes have received much less attention in kinetic studies, and relatively few studies have been published that can be used for mechanism validation. Fortunately, the few available sources are combined to describe the full set of n-alkanes included in this mechanism development, they cover most or all of the parameter ranges that are generally needed. These include shock tube ignition, rapid compression machine ignition, jet stirred reactors, flow reactors, and laminar flames, and they also cover a good variety of purely high temperature and lower temperature phenomena. We also found it very useful and interesting to combine groups of experimental data analyses and computed results to show a unified description of rapid compression machine, intermediate temperature and high temperature shock tube ignition.

High temperature shock tube ignition

Conventional, high temperature shock tube ignition of larger n-alkanes have been carried out by Davidson et al. [73,74], Zhukov et al. [75,76], Olchanski and Burcat [40], for n-decane, and the present n-alkane mechanism was used to simulate each of these studies. Larger hydrocarbons have rarely been studied in shock tube experiments, largely because the low volatility of the liquid fuels makes it difficult to prepare homogeneous gas-phase fuel/oxidizer mixtures. For these calculations with n-decane fuel, the portions of the full mechanism describing C_{11} - C_{16} kinetics were removed, making the calculations more efficient, as noted above.

Most of these studies measured only the ignition delay time, measured as functions of variations in initial reactant concentrations and initial post-shock unreacted temperature and pressure. However, Davidson et al. [73] also reported time-dependent OH radical concentrations during the ignition delay period, and Olchanski and Burcat [40] measured a number of reaction intermediates by quenching some shock tube ignition events, recovering the partially reacted mixtures and measuring their concentrations via gas chromatography. The measurements of reactive intermediates in both of these studies contributes a great deal of additional information that is very useful for mechanism validation.

High temperature shock tube experiments - 1

Olchanski and Burcat [40] investigated the shock tube ignition delay of mixtures of n-decane and oxygen, diluted in argon. Eight distinct mixtures containing 0.49% to 1.5% n-decane and 4.16% to 23.25% O₂ were included, with temperatures ranging from 1239K to 1616K and pressures from 1.82 to 10 atm. A total of 144 shocks were analyzed, and their paper includes specific, representative results from 30 of them.

Computed results with the present mechanism are compared with the experiments in Figure 2. The results for the richest mixture 7 at $\phi = 3$ are not shown, from which all four shocks in that group showed poor agreement, with the computed results igniting faster than the experiments by factors of approximately 10.

For the shocks shown in Fig. 2, the agreement between experimental and computed results is mixed, with some shocks providing very good agreement and others with only fair agreement with other shocks. In most cases, the computed ignitions are faster than in the experiments, with overall better agreement at lower temperatures than at the highest range of temperatures.

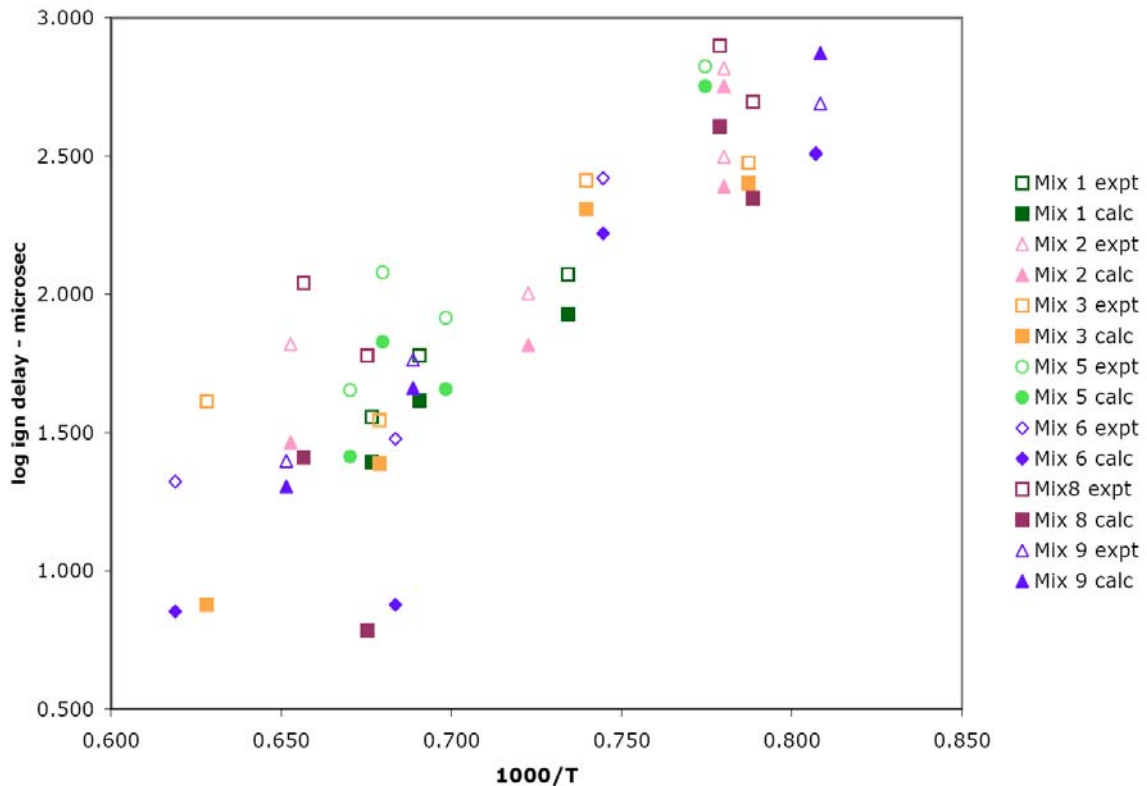


Fig. 2. Computed and experimental [40] ignition delay times for n-decane/O₂/Ar mixtures behind reflected shock waves. Experiments are shown as filled symbols, computed results as open symbols, so each shock is represented by a pair of symbols.

These simulations suggest that further attention is needed, including detailed kinetic sensitivity analyses, to help diagnose the differences. One difference is the criterion used to indicate ignition; in the calculations, ignition is determined when the reactive mixture exceeds the initial value by 300K, while in the experiments, the ignition delay is defined as “the time intervals between the rapid rise of the pressure due to the shock arrival and the onset of the pressure due to the ignition”. At constant volume, as assumed in the computations, the pressure and temperature track very closely, so the two definitions of ignition delay are generally close to identical.

High temperature shock tube experiments - 2

Frequently, reflected wave shock tube experiments of hydrocarbon ignition provide only ignition delay times for use in mechanism validation. These integrated measurements are useful but often are of limited value. Some researchers have recently added the capability of measuring selected radical concentrations during the ignition delay period, which provides a much more demanding test of a reaction mechanism. A recent study by Davidson et al. [73] measured OH concentrations during the shock tube ignition of n-decane, in addition to several smaller n-alkanes. We have used the present kinetic model to simulate those shock tube experimental results.

These shock tube experiments were carried out at temperatures from 1400K to nearly 1800K, very strongly in the high temperature regime for the kinetic schemes. Post-shock pressures were all about 2 atm, and the reactive mixtures are all close to stoichiometric and quite dilute in argon. Four groups of shocks were reported, three groups with 300 ppm n-decane at $\phi = 0.8$, $\phi = 1.0$ and $\phi = 1.2$, and a fourth stoichiometric group with 2000 ppm n-decane. A representative example of the measurements is shown as the dashed curve in Figure 3, with a negligible induction period, followed by a

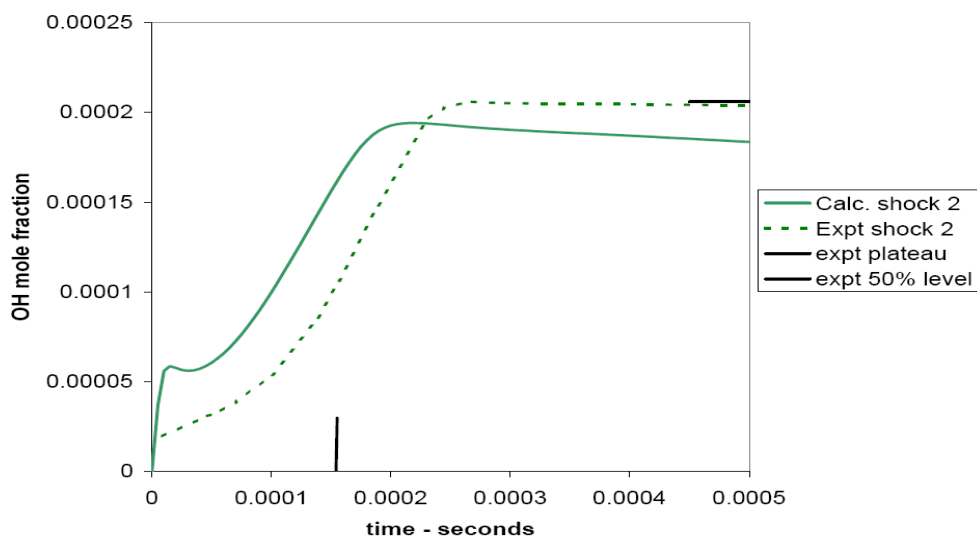


Fig. 3. Experimental [73] and computed OH mole fractions in n-decane ignition. $T_0=1525\text{K}$, $\phi = 1$, $n\text{-C}_{10}\text{H}_{22}$ initial concentration is 300 ppm.

fairly steep rise to a level of about 200 ppm at about 225 μs . The experimental results are characterized by the time at which the OH reaches half its maximum level, which is marked by the bar on the time axis at 154 ms. The second indicator is the final “plateau” level of the OH concentration, which is at 206 ppm, shown by the bar on the right hand side of the figure.

The results of the model simulation are shown as the solid curve on Fig. 3, which shows a slightly earlier rise in OH concentration followed by a rapid rise to a final level very similar to that measured experimentally. Two additional examples of these results are shown in Figure 4, one from each of the other groups of shocks.

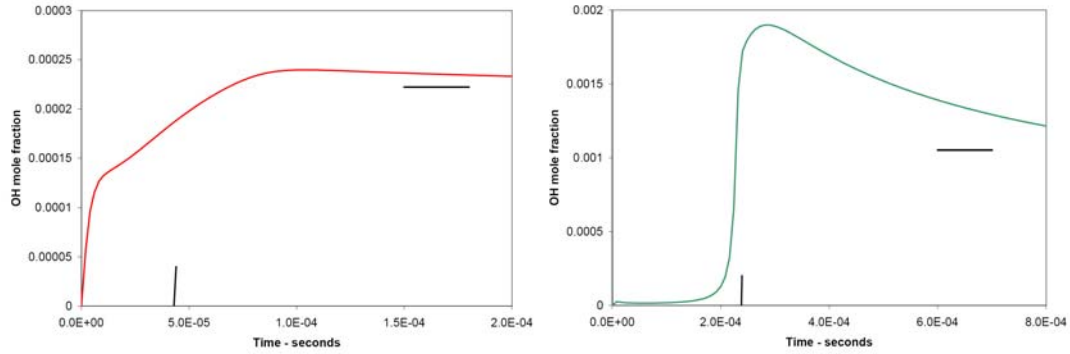


Fig. 4. Computed OH concentrations for (left) $T_0=1706\text{K}$, 300 ppm n-decane, $\phi = 1.2$, and (right) $T_0=1404\text{K}$, 2000 ppm, $\phi = 1.0$. Experiments from [73].

In the first case in Fig. 4, the model reproduces the midpoint of the rise in OH and the plateau value quite well. In the second case, the increased fuel content (i.e., 2000 ppm) produces enough energy to make the ignition very rapid, and the time of ignition is captured accurately by the model. In the same case, the OH overshoots its final value, and it is evident that the computed OH is falling towards its plateau value at a somewhat longer time scale than the end of the computation.

Intermediate temperature shock tube experiments

Intermediate temperature shock tube experiments have been carried out by the group in Aachen led by Adomeit, for mixtures of n-heptane and air [77] and, more recently, n-decane and air [78]. The n-heptane/air experiments were carried out at approximately 13.5 and 40 bars pressure and for stoichiometric, lean and rich fuel/air mixtures. The experiments for n-heptane /air have been very widely used to validate fully detailed and other reduced or skeletal kinetic mechanisms for n-heptane oxidation. The n-decane experiments, at pressures of 13 bars and equivalence ratios of 0.5, 1.0 and 2.0, and at 50 bars for equivalence ratios of 0.67, 1.0 and 2.0, have also been used for the same purposes of validation of recent mechanisms for n-decane/air kinetics.

The experiments, as illustrated in Figure 5, show a transition from low temperature to high temperature ignition, with a negative temperature coefficient (NTC) region between them. The n-heptane experiments demonstrated not only the NTC behavior but also the variation in NTC behavior with equivalence ratio and with pressure. In particular, increasing pressure and increasing equivalence ratio moved the ntc region to gradually higher temperatures, but they also reduced the magnitude of the ntc behavior.

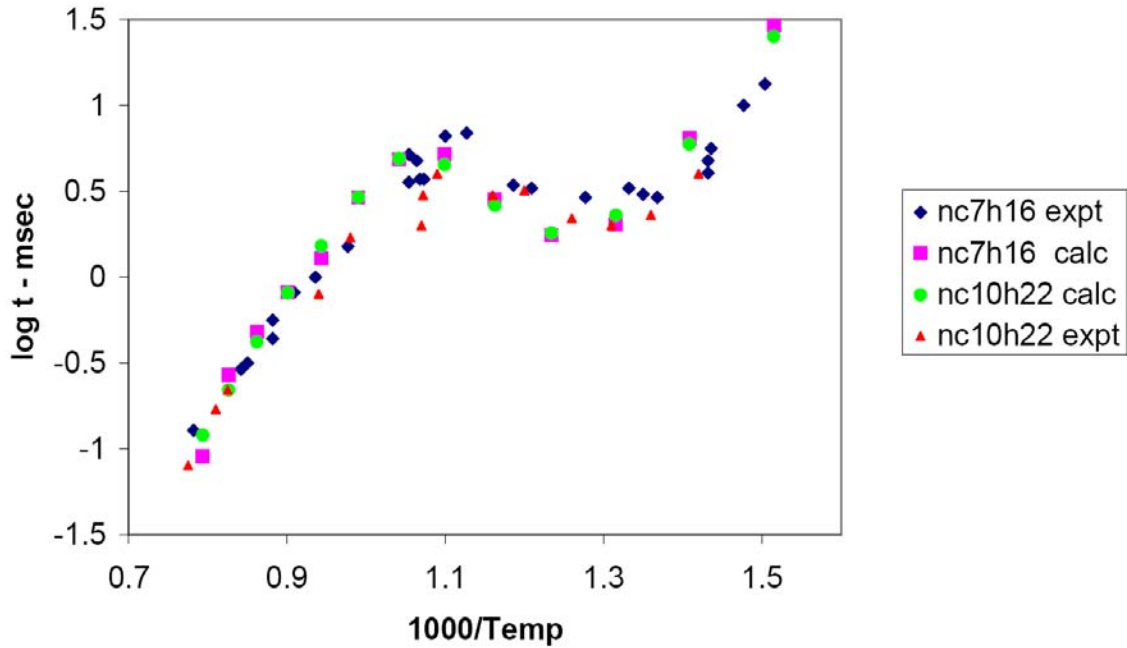


Fig. 5. Shock tube ignition delay times for n-heptane and n-decane, all at 13.5 bar pressure and stoichiometric fuel/air. Experiments are from Ciezki and Adomeit [77] and Pfahl et al. [78]. N-heptane computed results from ref [9].

Nehse et al. [39] examined these ignition results for both n-heptane and n-decane using a somewhat lumped kinetic mechanism, successfully reproducing the major features of the temperature and equivalence ratio variations for both fuels. Another very interesting result of Nehse et al. was that the computed ignition delay times for stoichiometric n-decane/air at 13.5 bar pressure were virtually identical to the results for n-heptane/air. Pfahl et al. noted the similarities between the ignition delays of these fuels but noted that the n-decane results had slightly shorter ignition delays at lower temperatures. Pfahl et al. also noted that α -methyl naphthalene did not show the NTC behavior of the n-alkanes and that dimethyl ether showed more rapid ignition than the n-alkanes at low temperatures. Other modeling studies in the rapid compression machine [79] have also used the n-decane experimental results for model validation and will be discussed below.

The experimental results for both stoichiometric n-heptane and n-decane mixtures in air at 13.5 bar are compared with computed results using the present kinetic mechanisms are plotted in Figure 5, showing very good agreement for both fuels. Similar close agreement was found for mixtures at 6.5 and 40 bar pressures and at equivalence ratios of 0.5 and 2.0 for n-heptane/air and 0.67 and 2.0 for n-decane. The higher pressure experiments are of particular value for mechanism validation because they address pressures encountered during ignition in diesel and HCCI engines and under knocking conditions in spark-ignition engines.

Although experimental results are available for comparison only for n-heptane and n-decane, we carried out a complete series of simulations at 13.5 bar initial pressure for each n-alkane from n-octane through n-hexadecane at stoichiometric conditions to see if all of them would show similar ignition behavior, and the results are shown in Figure 6. Within the limits of the calculations, each of the fuels shows virtually identical ignition delay times except for temperatures within the NTC region, where there is a slight but definite trend where the ignition delay time increases as the length of the n-alkane chain increases, with the most pronounced differences located at an initial temperature of about 810K.

This family of computed problems has some interesting features. For each n-alkane from octane to hexadecane, the mixture is stoichiometric in air. One n-octane molecule has only half the number of C atoms as n-hexadecane, with nearly the same ratio of H atoms as well, so the amount of air required to consume a molecule of n-octane is only approximately half that required to consume a molecule of n-hexadecane. For both fuels, a stoichiometric mixture is nearly all air, with only a very small amount of fuel. For example, the present n-octane/air mixture contains 98.35% air and only 1.65% n-octane, while the n-hexadecane/air mixture contains 99.15% air and 0.85% n-hexadecane. The initial compositions of the other stoichiometric n-alkane/air mixtures vary monotonically between these two limits, they will all be approximately 99% air and between 0.85% and 1.65% fuel. While these all contain nearly equal amounts of air, and therefore equal amounts of oxygen as well, there are twice as many n-octane molecules

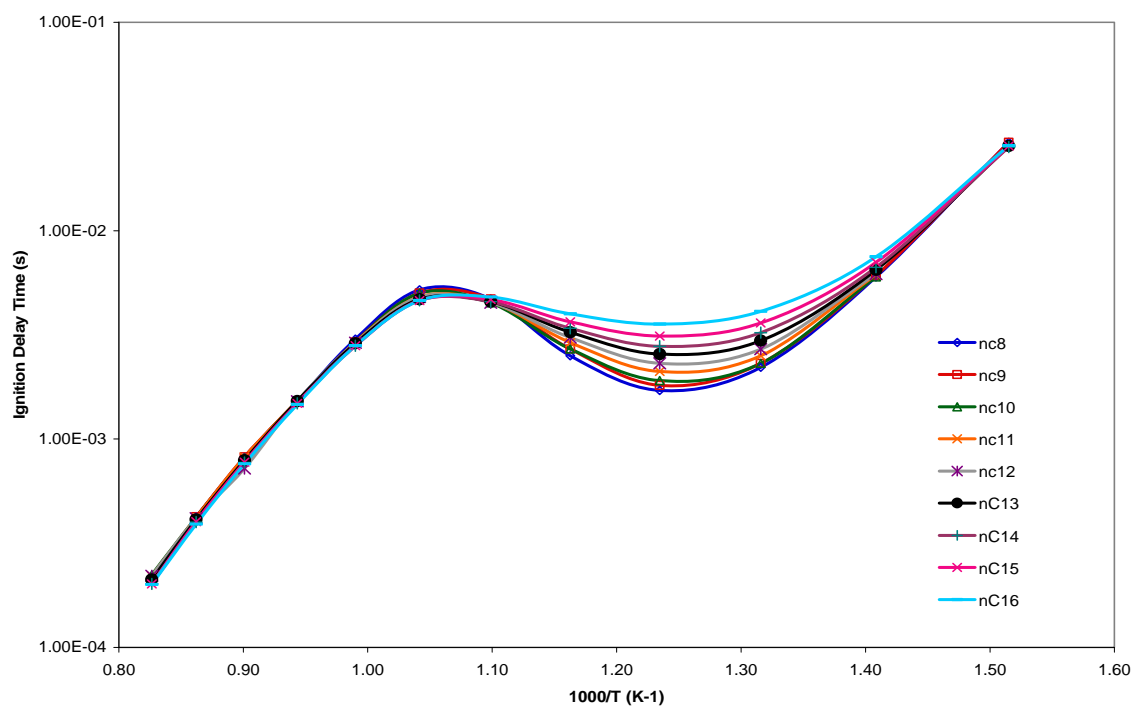


Fig. 6. Computed ignition delay times for stoichiometric n-alkanes at 13.5 bar.

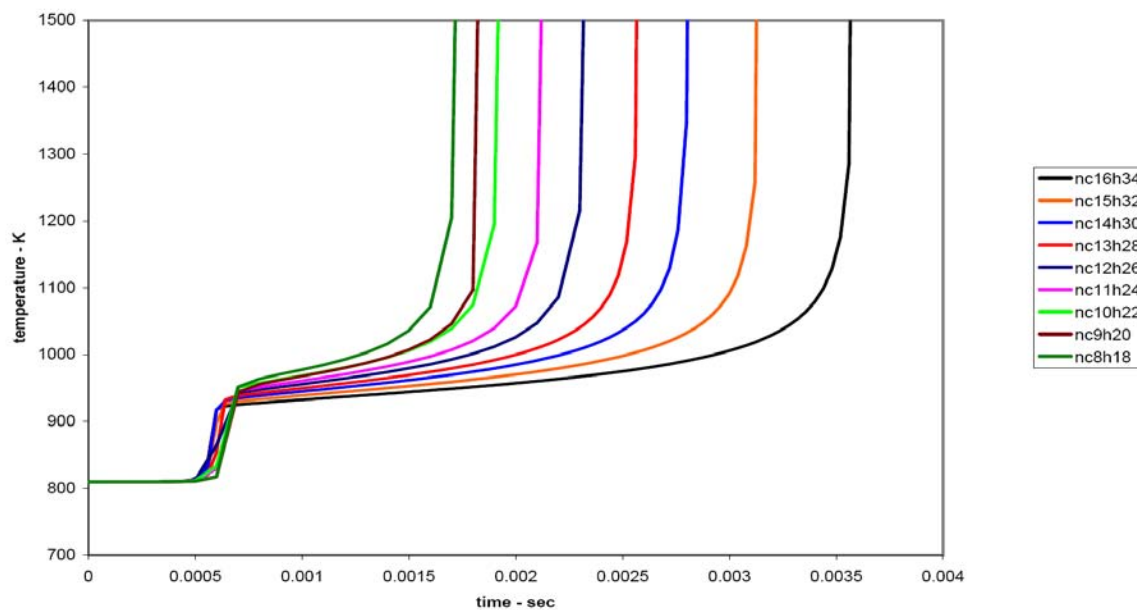


Fig. 7. Computed temperatures for ignition of n-alkanes from n-octane to n-hexadecane, showing two-stage ignitions.

as n-hexadecane molecules in their respective stoichiometric fuel/air mixtures. The physical properties of all these mixtures are almost completely determined by the properties of air, but their chemical properties are controlled entirely by the kinetics of the different fuels. As our present example will show, these differences in initial compositions will be the key to explaining the behavior of these systems.

The computed temperatures in these simulations during ignition are shown in Figure 7, showing a two-stage ignition with each fuel. The first stage ignitions begin at the same time and ends at about the same temperature for each fuel, and the computations indicate that this “plateau” temperature is determined from the equilibrium of the $R + O_2 = RO_2$ reactions. Since all of these fuels are dominated by secondary C - H bonds, this similarity in plateau temperature is not surprising. The onset of the second, final stage of ignition increases monotonically with the length of the n-alkane chain. This is somewhat surprising, since the cetane number of these alkanes increases from n-octane to n-hexadecane, and since cetane number is viewed as an indication of the ignition quality or ignition timing of these fuels, it might appear that these fuels should ignite in the order of cetane number rather than the reverse order shown in Figs. 6 and 7. However, the ignition of diesel fuel that determines cetane ratings has been shown by Dec [80] to involve ignition at very fuel-rich conditions ($\phi \sim 3-4$), not at the stoichiometric conditions as those shown in Figs. 6 and 7. Further ignition studies using the present mechanisms under relevant rich conditions are needed to address this question.

The corresponding amounts of fuel consumption during the first stage of ignition are plotted in Figure 8, showing very clearly that the fractional amount of fuel consumption is smallest for n-octane and largest for n-hexadecane. Specifically, the initial mole fraction of n-octane is 0.0165, and after the first stage, its mole fraction is 0.006, a reduction of 64%. The corresponding reduction in n-hexadecane is from an initial mole fraction of 0.0085 to a lower level of 0.0006, a reduction of 93%, and the reductions in levels of the other n-alkanes vary monotonically between these limits. At

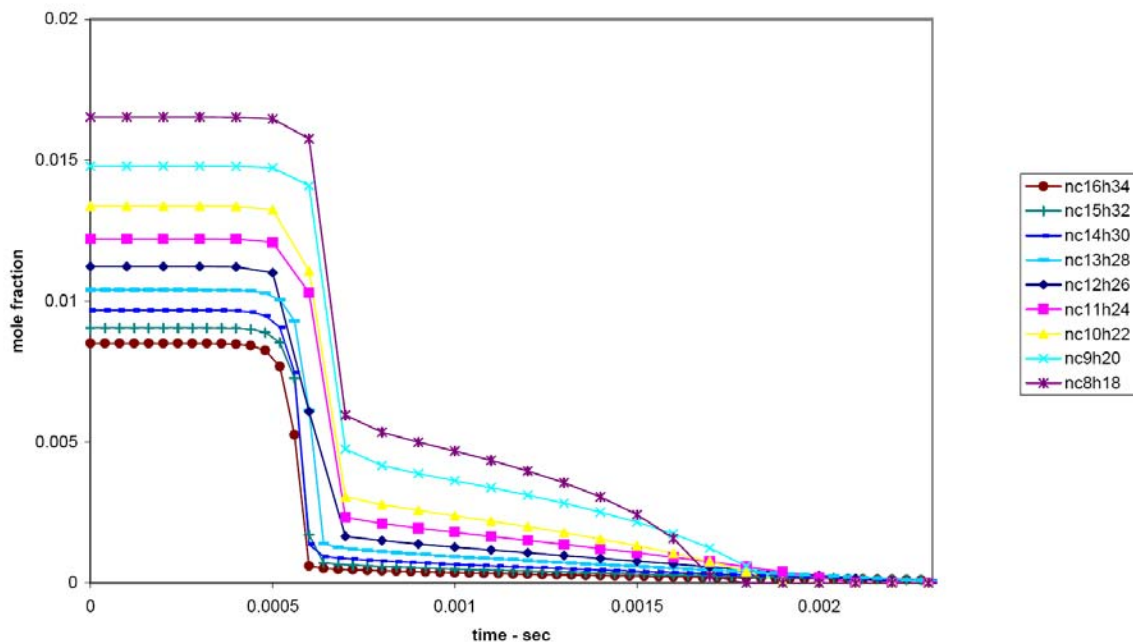


Fig. 8. Consumption of fuel during the first ignition stage for n-alkane fuels. Initial temperature in each case is 810K, 13.5 bar pressure, at stoichiometric conditions in air.

first glance, it is perhaps surprising to see that n-octane ignites considerably earlier than n-hexadecane and all of the other n-alkanes larger than n-octane, in spite of the fact that much more n-octane remains after the first stage than any of the other n-alkane fuels.

However, the absolute amounts of n-octane consumed during the first stage are larger than the absolute amounts of n-hexadecane consumed. For n-octane, the reduction from its initial mole fraction of 0.0165 to 0.006 produces 0.0105 mole fraction units of octyl radicals, while n-hexadecane produces only 0.0079 mole fraction units of hexadecyl radicals, with the intermediate n-alkanes producing intermediate amounts of alkyl radicals. All these trends are results of the fact that these are stoichiometric mixtures of n-alkanes with air, and the initial n-octane concentration is twice that of n-hexadecane.

At the elevated pressures of these shock tube experiments (13.5 bar), the low temperature regime for hydrocarbon oxidation is at its peak of activity at 810K, the initial temperature for each calculation shown in Figs. 6 and 7. It is also the temperature at which the NTC region begins, as shown in Fig. 9. Under these conditions, the low temperature alkylperoxy radical isomerization reaction pathways are responsible for most of the chain branching that produces the first stage ignition. Each alkyl radical can produce, at most, one low temperature reaction chain, regardless of the length of the carbon chain in the alkyl radical. As a result, because more octyl radicals are produced overall from the much larger amounts of initial fuel molecules than hexadecyl radicals, there is more low temperature reactivity for n-octane than for n-hexadecane. These

differences continue at lower rates after the end of the first stage of ignition. Thus the rate of n-octane oxidation is greater at every stage of the reaction than the rate of n-hexadecane oxidation, leading to the earlier ignition of the n-octane. Larger numbers of n-octane molecules in the fuel produce larger numbers of alkyl radicals and more chain branching via low temperature oxidation kinetics than in n-hexadecane oxidation under the stoichiometric conditions of these experiments and calculations.

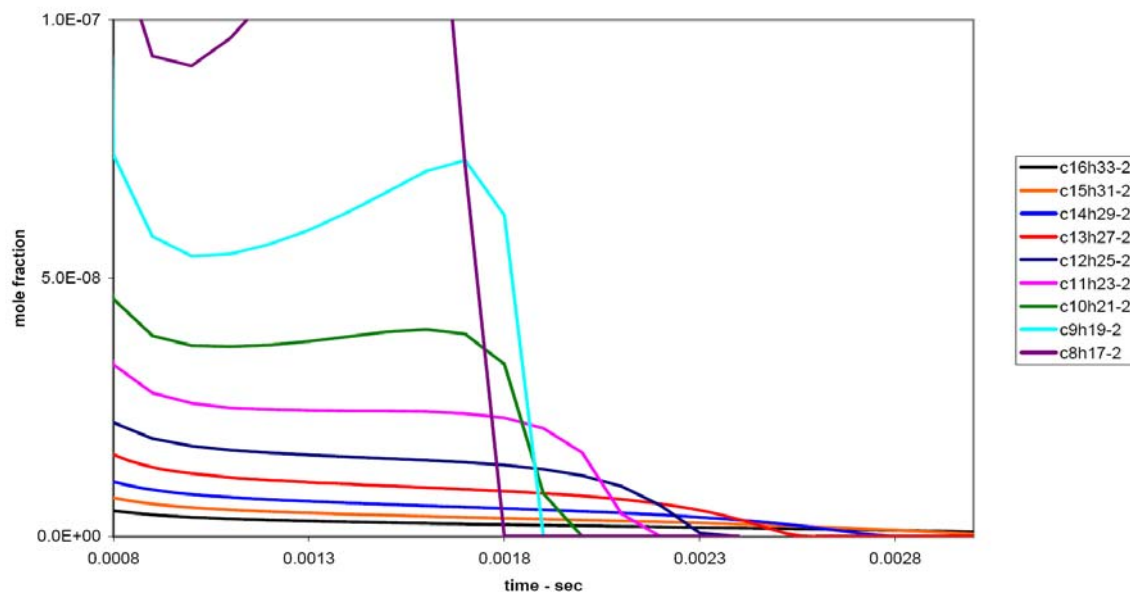


Figure 9. Computed 2-alkyl radical concentrations following first stage ignition for a series of n-alkanes.

Rapid compression machine experiments

The low and intermediate temperature regime for hydrocarbon oxidation is often studied experimentally in the rapid compression machine (RCM). Typical temperatures in RCM experiments are from about 650K and 900K, which spans the negative temperature coefficient (NTC) region which has important implications for hydrocarbon ignition in internal combustion engines. Many laboratory groups have studied systems in the RCM, including current groups in Leeds, Lille, Michigan, MIT, Galway, and Case. All of these groups have addressed fuels closely related to the large n-alkanes of concern in this paper, but only the group of C. J. Sung at Case Western Reserve University have carried out experiments [79] specifically with n-decane. The large n-alkanes present significant challenges for careful experiments in most facilities because their vapor pressures are quite low, making it difficult to vaporize sufficient fuel for problems intended to operate at room temperature and pressure. The usual solution for this difficulty is to begin operation at elevated temperatures (e.g., Zhao et al. [42]) to provide more vaporized fuel, but that can raise safety problems and makes it difficult to relate experimental results to other fuels studied at room temperature.

In the Kumar et al. experiments [79], vaporized mixtures of n-decane, oxygen and diluent are mixed at an equivalence ratio of 0.8. Precompressed gas mixture temperatures are varied in order to achieve a range of compressed temperatures, and these gases are then compressed rapidly to pressures in the range from 7-30 bar and temperatures of 630-706K. The experiments use a novel piston design to remove as much as possible of the boundary layer gases that form during the compression stroke and make the determination of the post-compression gas mixture temperature especially difficult. The post-compression ignition delay times were measured and compared with computed results using a reaction mechanism developed by Bikas and Peters [40]. The general trends in the experiments were reproduced qualitatively well by that mechanism, but the actual ignition delay times from the model were consistently longer than the corresponding experiments by factors of 4 - 5. For example, at a compressed pressure of 30 bar and temperature of 662K, the measured ignition delay was 4.5 ms while the calculated ignition delay was about 22 ms. Kumar et al. do not address the reasons for the significant differences between their measurements and the modeling predictions, but use the term “over-prediction” when summarizing the computed values.

We repeated the ignition delay simulations using the present n-alkane mechanism, and a series of results over a range of compressed gas initial temperatures at 14.3 bar pressure is shown in Figure 10. The results show a familiar pattern of two-stage ignitions for compressed gas temperatures of 680K to 740K. As observed by Kumar et al., these

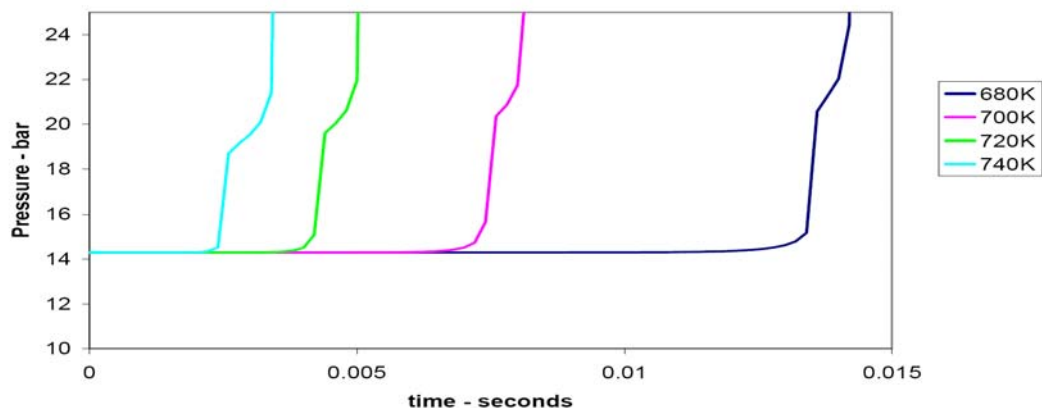


Fig. 10. Computed pressures in RCM experiments at 14.3 bar pressure

computed results did not show any NTC behavior, which would be expected at temperatures higher than those represented in the experiments.

Interestingly, our computed results were in generally better agreement with the computed results using the Bikas and Peters mechanism for n-decane than they are with the experimental results. The three sets of results are summarized in Fig. 11.

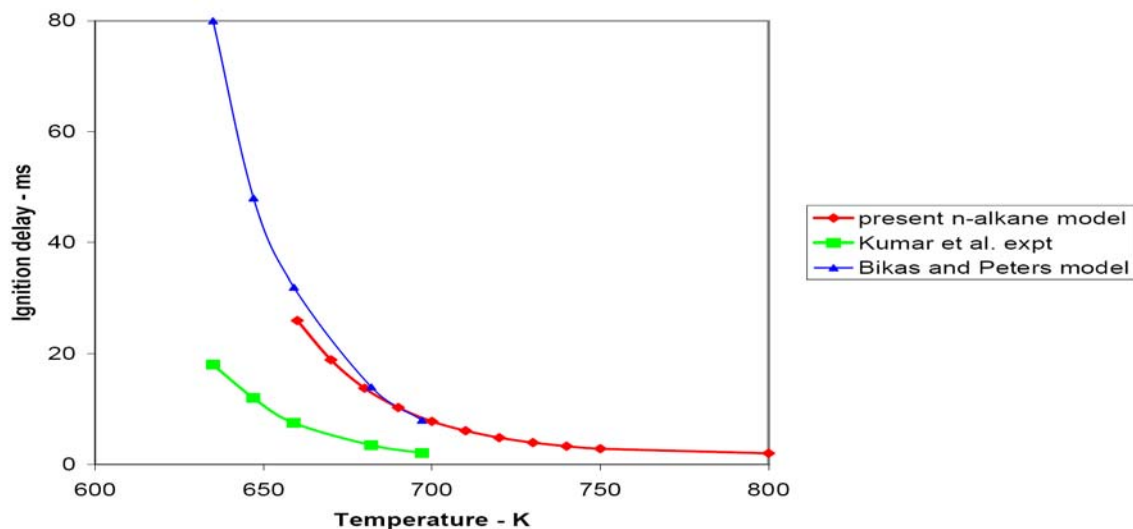


Fig. 11. Computed and experimentally measured ignition delay times for n-decane/air at $\phi = 0.8$ and 14.3 bar pressure.

Kumar et al. then adopted a very interesting approach for data analysis, combining their RCM experimental results with the intermediate temperature shock tube experiments for n-decane by Pfahl et al. [78] and of Zhukov et al. [76]. The assumption is very common and well accepted that essentially no reaction occurs in the shock tube

until the extremely rapid rise in temperature and pressure with the shock arrival, but the compression stroke, achieving similar temperatures and pressures as in the shock tube, occurs over a much longer period of time in the RCM. However, if it is assumed that no reaction occurs during the compression stroke, then it is logical to conclude that RCM and shock tube ignition delay times at the same temperature and pressure and equivalence ratio ought to be equal.

Exactly the same concept was used very recently by Peterson et al. [81] when they intercompared shock tube and RCM ignition delay measurements for propane ignition. In the case of Peterson et al., the RCM data and several sets of shock tube results showed excellent agreement, but two shock tube studies showed results that were inconsistent from the rest, and on that basis, Peterson et al. went on to question the reliability of the inconsistent set of shock tube results.

Following the examples of Kumar et al. and Peterson et al., we have plotted together several sets of data for the ignition of n-decane/air at about 14 bar initial pressure on Figure 12. The experimental results of Kumar et al. and the computed results using the Bikas and Peters mechanism were originally obtained at an equivalence ratio of 0.8, while the present model results and the shock tube results of Ciezki et al. [77] and Pfahl et al. [78] were obtained for stoichiometric mixtures. We carried out computations

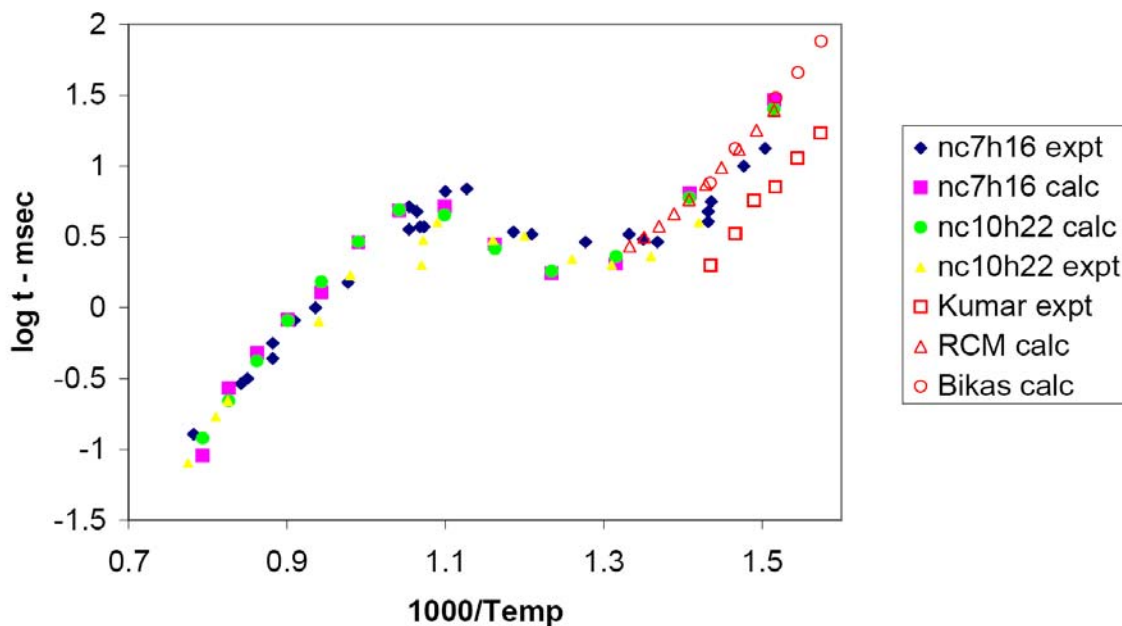


Fig. 12. RCM ignition delay times for n-decane experiments of Kumar et al. [79] and kinetic model results, scaled from $\phi=0.8$ for comparison with stoichiometric experiments [77,78] and computed results discussed above. Computed RCM results are open triangles, experimental RCM results are open squares. Results for n-heptane are also included.

at $\phi = 0.8$ and 1.0 and pressures of 14 bar, finding that the ignition delay times for the stoichiometric conditions were about 5% shorter than at $\phi = 0.8$. As a result, the experimental results from Kumar et al. and the computed results using the Bikas and Peters mechanism at $\phi = 0.8$ were reduced by 5% and then plotted in Fig. 12. In addition, experimental shock tube ignition delay times at 14 bar pressure and stoichiometric mixtures of n-heptane/air were also included in Fig. 12. As discussed earlier, the shock tube ignition delays for all of the n-alkanes from C_7 to C_{16} are remarkably similar over nearly all of the temperature range in Fig. 12, so inclusion of the n-heptane/air modeling and experimental results provides additional calibration of the experimental and kinetic modeling results.

When the experimental results of Kumar et al. are compared with the computed and experimental results for the shock tube ignition of n-decane and n-heptane, it is clear from Fig. 12 that the results of Kumar et al. are slightly faster than all the other results. If we believe that the results should be internally consistent, then there must be some reason for the faster ignition of n-decane in the RCM experiments. We examined one possible explanation; it is likely that n-decane reacts to some extent during the last few milliseconds of the compression stroke, which would lead to experimental results for the ignition delay time that are too short. We carried out calculations for the last portion of the compression stroke and found that some, but not all, of the differences between the Kumar et al. and the other results for ignition delay could be attributed to their neglect of reaction during the compression stroke. Past studies of RCM ignition of n-heptane [82] showed considerable amounts of fuel consumption during the compression stroke in the Leeds University RCM, which has a relatively rapid compression stroke. Slower compression strokes would make this effect larger. There is also some experimental variation in the measurements in both the RCM and the shock tube that might produce some disagreement. The novel construction of the Case RCM, to reduce the effects of wall boundary layers on the ignition, may also not yet be fully understood and may be contributing to the uncertainties. Further comparisons between the Case RCM and results from other RCM facilities with fuels for which reliable kinetic mechanisms exist, are recommended to resolve some of these effects.

High temperature shock tube experiments - 3

Zhukov et al. [75,76] reported results of experiments determining the ignition delay times for stoichiometric and lean mixtures of n-decane in air behind reflected shock waves. Stoichiometric mixtures at 13 and 80 atmospheres pressure and lean ($\phi = 0.5$) mixtures at 78 atm. were included. Zhukov et al. compared their experimental ignition delay times with those of Pfahl et al. [78] with generally good agreement, at both 13 and 80 atm pressures. The measured ignition delay times were compared with computed values, using four different reaction mechanisms using EXGAS [25-29], Bikas and Peters [13], Lindstedt and Maurice [47,48] and Zhao et al. [42,43]. The mechanism of Zhao et al. was unsuccessful in reproducing the experimental results, due to the lack of low temperature reaction pathways which are important at the conditions of the experiments, and the other mechanisms provided results that were judged inaccurate by Zhukov et al., largely due to computed ignition delay times that were too long.

We used the present n-alkane mechanism for n-decane to simulate the shock tube experiments of Zhukov et al. The results at 13 atm pressure, for stoichiometric mixtures of n-decane and air, are summarized in Fig. 13. Similar to the model results reported by Zhukov et al., our computed ignition delay values appeared to be longer than the measured results by factors about 1.5, with a much larger difference for the lowest temperature point.

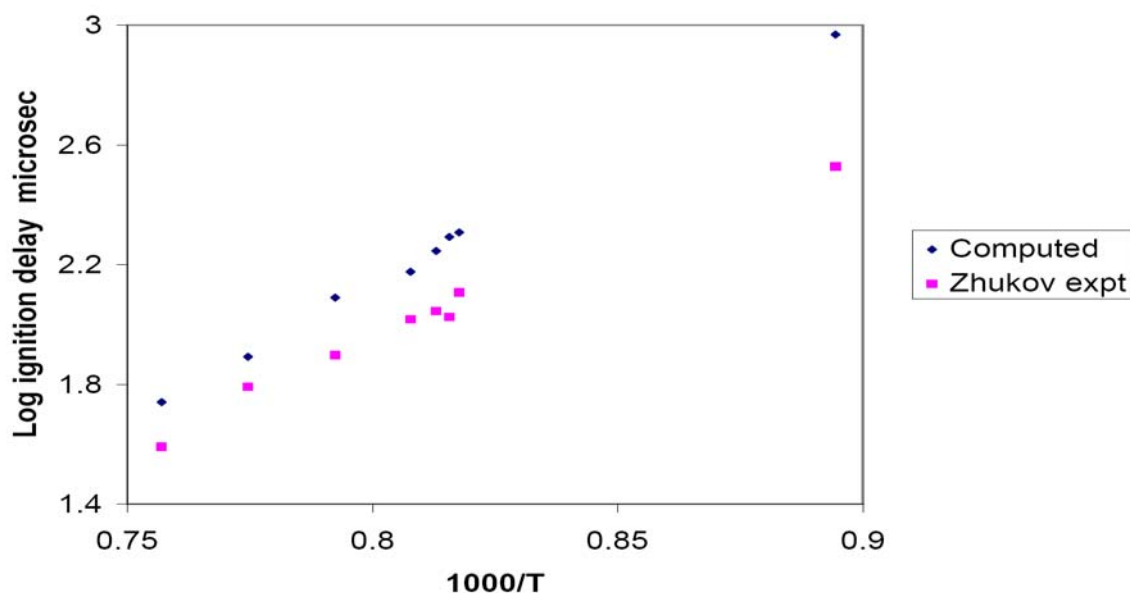


Fig. 13. Computed and experimental ignition delay times for $\phi = 1$ n-decane/air at 13 atm pressure. Experiments from Zhukov et al. [75,76]

Similar results were obtained for the higher pressure (~ 80 atm) experiments for $\phi = 0.5$ and 1.0, shown in Figures 14 and 15. In all three cases, it appears that the computed results are longer than the measured values by a modest margin.

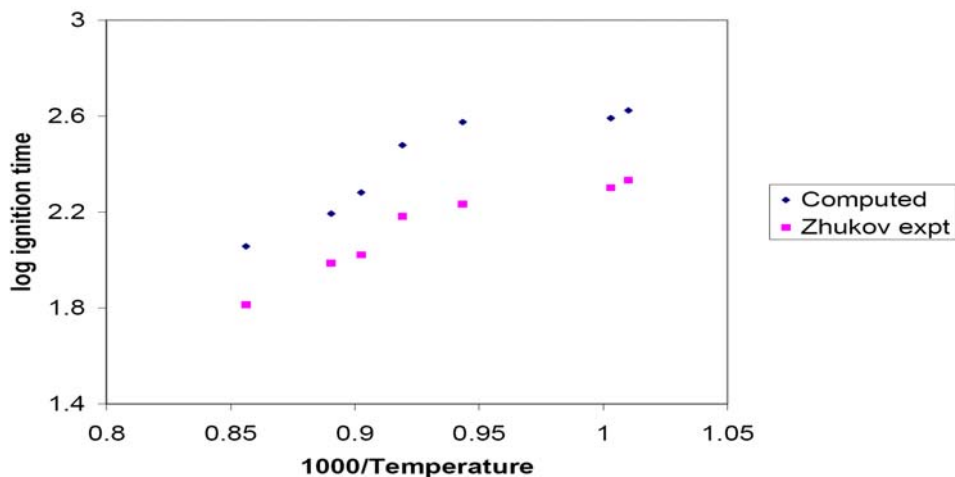


Fig. 14. Computed and experimental ignition delay times for $\phi = 0.5$, n-decane/air at 80 atm pressure. Experiments from Zhukov et al. [75,76]

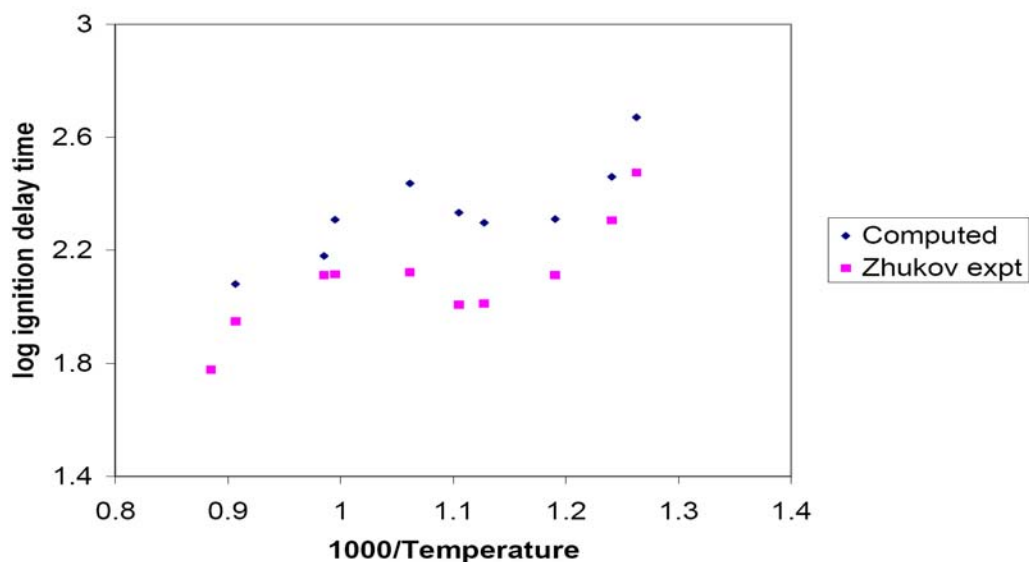


Fig. 15. Computed and experimental ignition delay times for $\phi = 1.0$, n-decane/air at 80 atm pressure. Experiments from Zhukov et al. [75,76]

In order to put the shock tube results of Zhukov et al. into context with the other high pressure shock tube and RCM ignition experiments and modeling results, we included the Zhukov et al. data into the same plot as in the analysis above for the other experiments, as shown in Fig. 16 with all the data measured at approximately 13-14 bar and, in the cases of Kumar et al. [79] and calculations of Bikas and Peters [13], extrapolated slightly from $\phi = 0.8$. The experiments of Zhukov et al. and the computed ignition delay times, using the present n-alkane mechanism, are shown at the highest extent of the temperature range covered in Fig. 16. At this degree of analysis, it appears

that the experimental results of Zhukov et al. are well within the expected ranges established by all of the other experiments and model calculations. The differences between modeling calculations and the individual Zhukov et al. measurements in the other figures above are evidently not significant. Although not shown in Fig. 16, it also

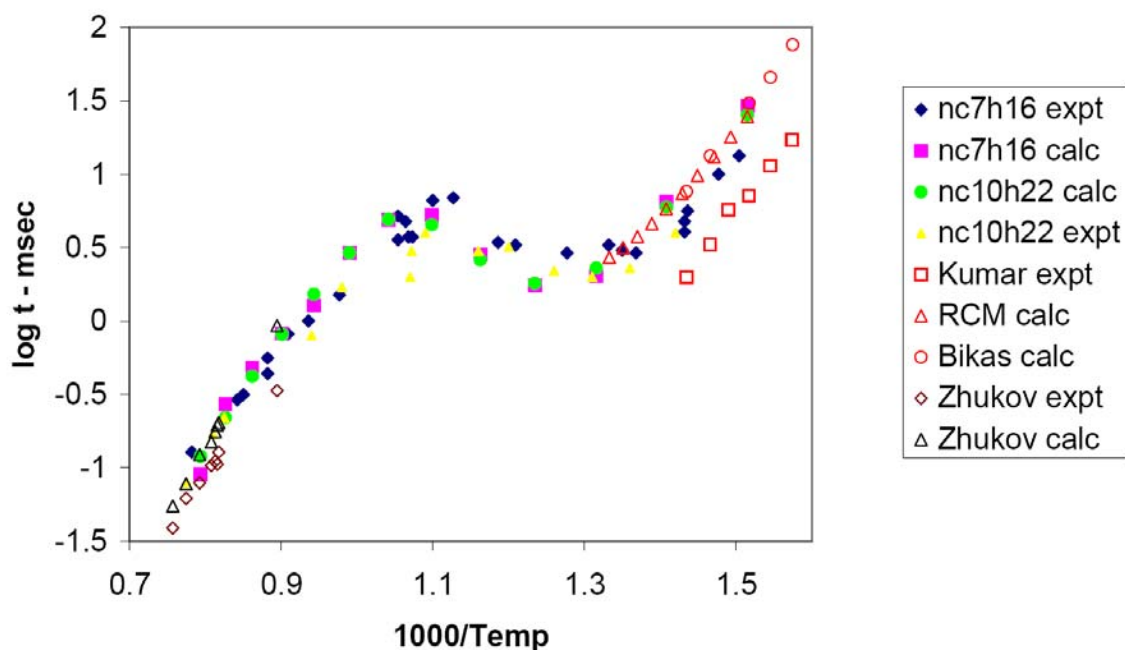


Fig. 16. Comparisons of experimental and computed ignition delay times for n-heptane and n-decane from a variety of experimental and kinetic modeling studies.

appears that the computed results reported by Zhukov et al., using reaction mechanisms from Bikas and Peters [13] and Lindstedt and Maurice [47,48] at 13-14 bar pressure, are also within the scatter of data at the highest temperatures plotted in Fig. 16, in spite of the discouraging comments of Zhukov et al.

The conditions are somewhat different for the higher pressure ignition experiments of Zhukov et al. The experimental results at $\phi = 1$ and 80 bar pressure are summarized in Fig. 17, together with the computed results from the present n-alkane mechanisms. Also shown are the experimental results from Pfahl et al. [78] at 50 bar pressure and $\phi = 1$ and the corresponding computed results, again using the present n-alkane mechanism. The two sets of experimental results are distinctly different, with ignition being faster as the pressure increases. In addition, the amount of NTC behavior seems to decrease as pressure increases, although the temperature range over which NTC behavior is observed seems to be nearly the same at 50 bar as at 80 bar. The trend toward faster ignition at higher pressure, and that the NTC region does not change significantly from 50 to 80 bar, appear to be reproduced by the kinetic mechanism quite well.

However, at both pressures, the computed results are longer than the experimental values by about a factor of 2. These high pressure ignition curves do not converge to a single overall picture such as that for 13 bar pressure in Fig. 16. As a result, we must

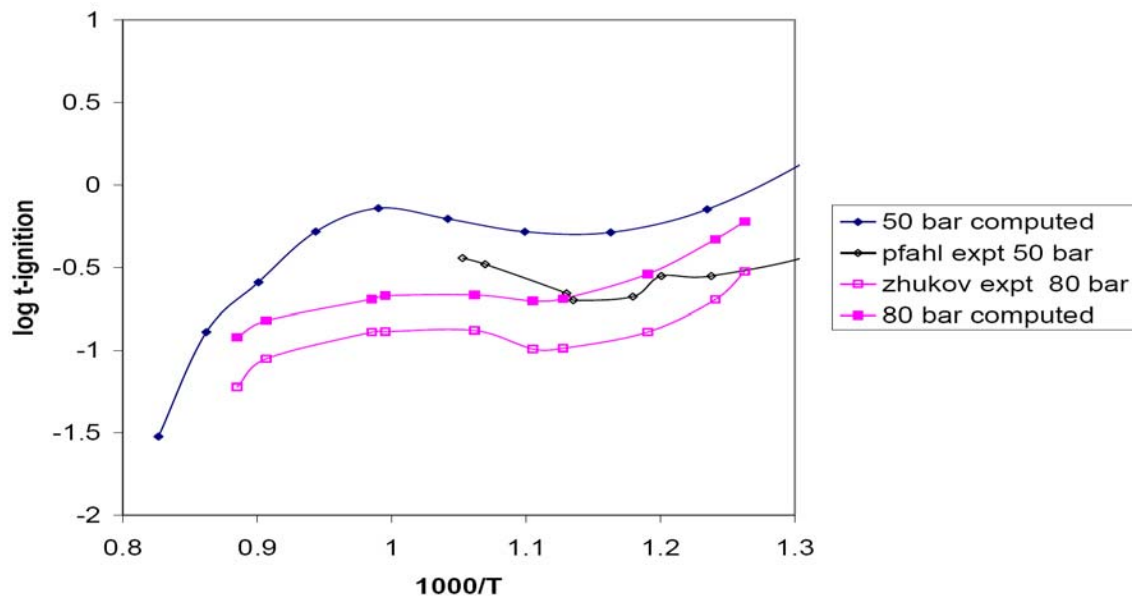


Fig. 17. Comparisons of shock tube experimental and computed ignition delay times of Zhukov et al. [71,72] at 80 bar and Pfahl et al. [74] at 50 bar, for n-decane at $\phi=1$.

conclude that the kinetic mechanism does not correctly reproduce the observed pressure dependence of these ignition events, and further study of the pressure dependence of the important reaction pathways is required. Additional experimental studies would be particularly valuable.

Flow reactor experiments

Zhao et al. [42,43] carried out pyrolysis and oxidation experiments for n-decane in the Princeton flow reactor at atmospheric pressure, measuring a wide range of intermediate and product concentrations as functions of time. They also produced reduced and skeletal kinetic mechanisms that did a very respectable job of reproducing many of the species levels. These measurements are very useful for mechanism validation of the present mechanism.

The pyrolysis experiment used 1456 ppm n-decane in nitrogen at an initial temperature of 1060K and found ethene, propene and larger 1-olefins as major products, in addition to methane, ethane and acetylene. The computed species concentrations for n-decane and the major products are shown in Figure 18. Comparisons between experiments and measurements are also excellent for methane and 1,3-butadiene, while computed results are lower than the experiments by a factor of 2 for 1-butene and higher than the experiments by a factor of 2 for 1-pentene.

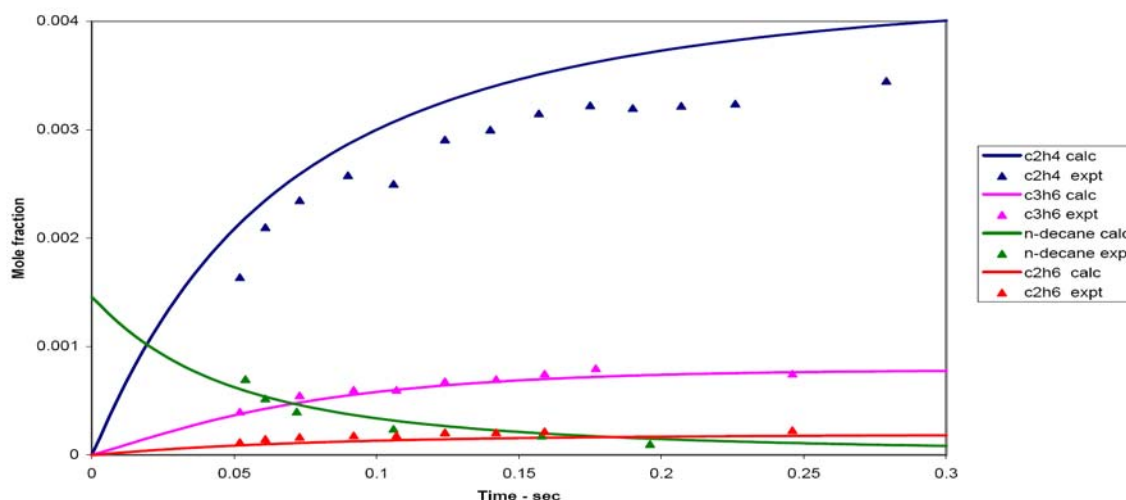


Fig. 18. Fuel and major pyrolysis products of n-decane in the Princeton flow reactor [42,43]. Lines show computed results, symbols show experimental results.

Comparisons between computed and experimental results for an oxidation case are shown in Figures 19 and 20. The mixture is stoichiometric and dilute, with 1452 ppm n-decane, at an initial temperature of 1019K and 1 bar pressure. The major products are ethene, carbon monoxide, 1-butene, propene, methane, 1-hexene, ethane and 1,3-butadiene, and the model shows good agreement with experimental results, except for CO, with the computations showing an earlier rise in CO concentration than in the experiments. We note that the skeletal mechanism of Zhao et al. [42,43] showed the same rise in CO concentrations earlier than the experimental results as shown in Fig. 19.

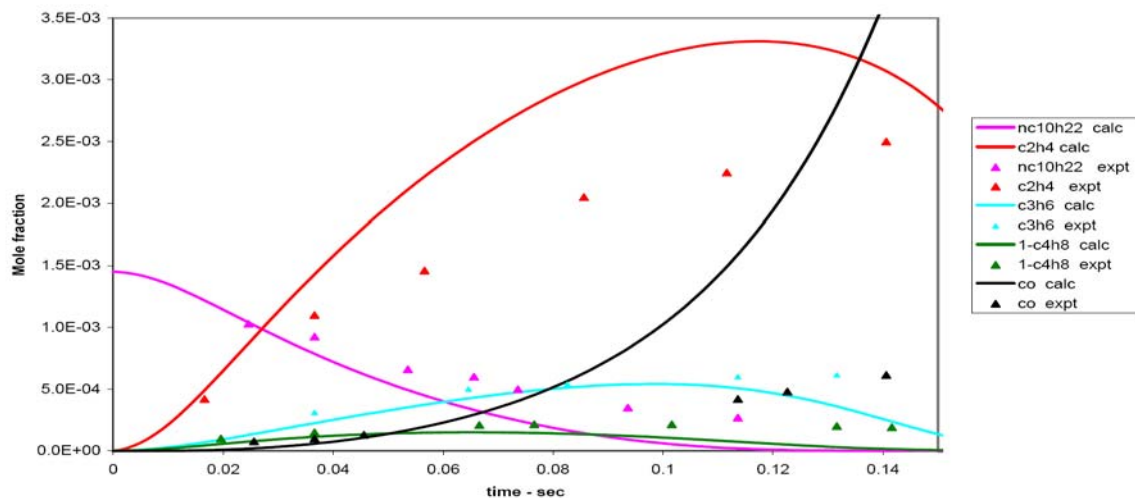


Figure 19. Major species concentrations for n-decane oxidation. Lines show computed results, symbols show experimental results [42,43].

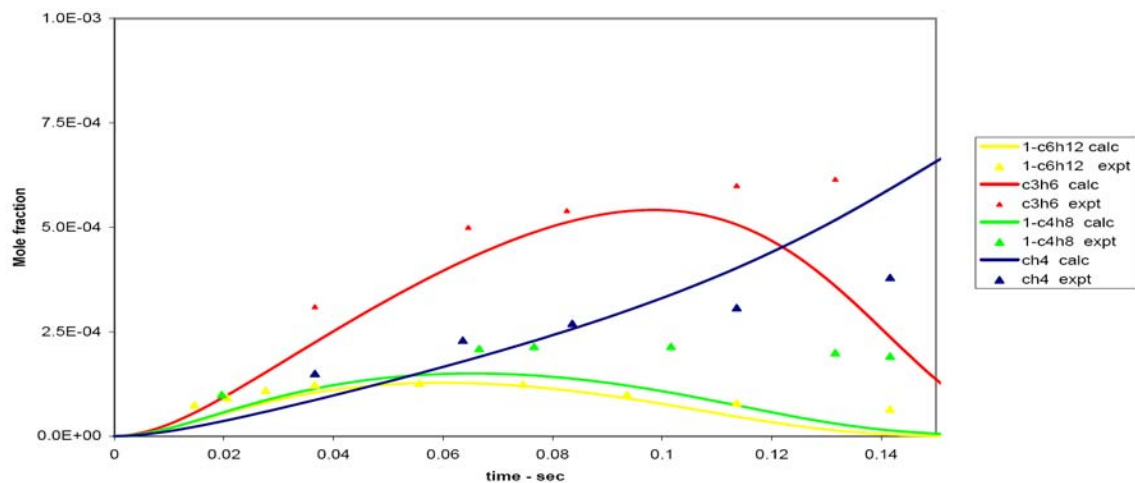


Figure 20. Intermediate species concentrations in n-decane oxidation. Lines show computed results, symbols show experimental data [42,43].

Kinetics in the transition temperature range between 900K and 1100K where the Princeton and other flow reactors have made such significant contributions, between the

low temperature alkylperoxy radical reaction regime and the high temperature regime controlled by H atom reactions with molecular oxygen and alkyl radical decomposition, is characterized best as a region in which the HO_2 radical exerts a particularly strong influence.

Jet stirred reactor experiments

Dagaut and collaborators have carried out an extensive series of experimental and kinetic modeling studies of oxidation of large hydrocarbons in a jet-stirred reactor, measuring many intermediate species concentrations over broad ranges of operating conditions that are very useful for kinetic mechanism development and validation. In particular, studies of n-decane [31] and n-hexadecane [29,30] have been carried out to test high temperature reaction mechanisms for these fuels. Later, those kinetic mechanisms for n-decane and n-hexadecane were used to test the surrogate capabilities of those fuels to describe oxidation of kerosene and biodiesel fuels. Overall, the n-alkanes appeared to be very satisfactory as surrogates for the practical transportation fuels.

Dagaut and Cathonnet [49] have reviewed experiments and modeling for the combustion of kerosene, showing how n-decane was used for some time as a suitable surrogate for kerosene. They showed that the overall reactivity of kerosene is due to its large n-alkane fraction, so if the function of the surrogate is limited to simulation of the kerosene, then n-decane is a good substitute. However, n-decane was later replaced by a variety of multicomponent mixtures that include large alkyl benzenes and are able to reproduce the production of benzene and other small aromatic intermediates and the formation of soot under some conditions. The role of large aliphatic compounds in kerosene, other jet fuels, and diesel fuel is still very important for ignition and energy release simulations, and the jet-stirred reactor experiments of Dagaut et al. are important for mechanism validation of several different large n-alkanes.

In the present work, experiments with n-decane and n-hexadecane oxidation are used to test the capabilities of the present n-alkane reaction mechanisms. For n-decane, experimental results are available for pressures at 1, 10, 20 and 40 atm, equivalence ratios from 0.2 to 1.5, residence times from 0.1 to 1.0 seconds, and a number of inlet concentrations of n-decane. In order to keep the reaction from proceeding too rapidly and forming flames or exploding, the total mixture is kept very dilute. For illustration and to demonstrate the level of mechanism validation that is possible with these experiments, we shall show comparisons between experimental and computed results for one stoichiometric mixture at 10 atm pressure and three additional cases for lean, stoichiometric and rich mixtures at atmospheric pressure.

The first test was reported by Dagaut et al. [32] in a study of kerosene combustion at pressures from 10 to 40 atm pressures, in which n-decane was used as a surrogate for the kerosene for kinetic modeling purposes. The kinetic model was intended for high temperature systems and reproduced the observations quite well for most species n-decane. The first specific example used here is intended to show the mechanism capabilities at elevated pressures and describes a dilute (1000 ppm fuel) stoichiometric mixture of n-decane and oxygen, at 10 atm pressure and a residence time in the stirred reactor of 0.5 seconds. Figure 21 shows the computed and experimental values for 5 species for which measured values were reported, with good agreement between model and experiment.

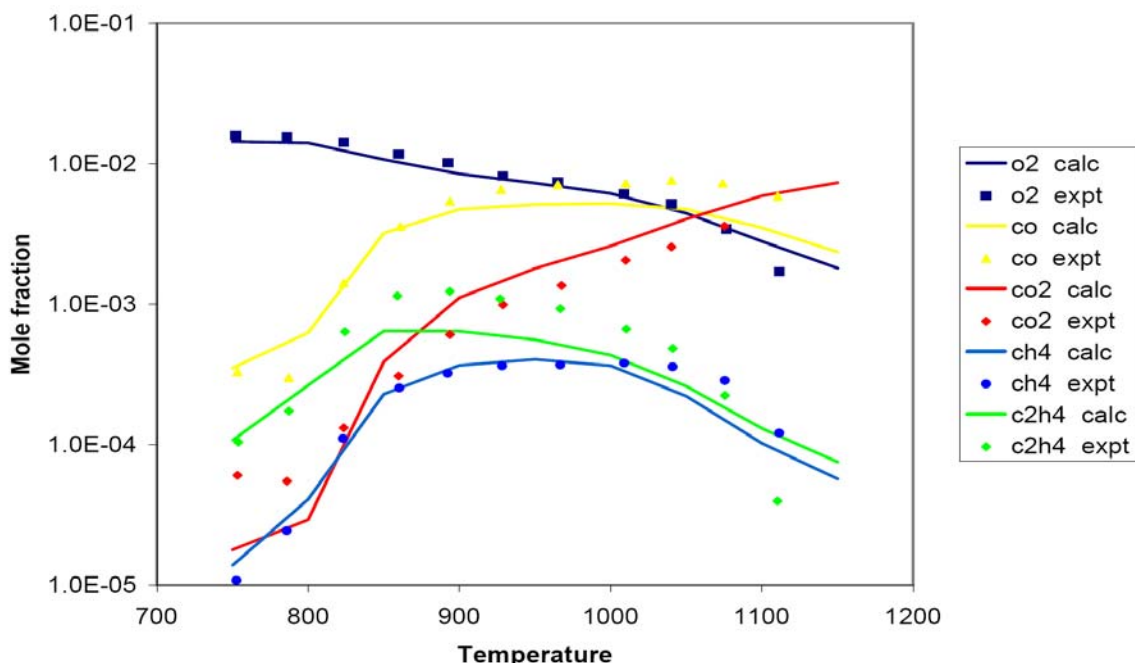


Fig. 21. Chemical species concentrations in a jet stirred reactor. Lines represent computed values, symbols are experimental results [32].

Other interesting kinetic information from this simulation includes the relative levels of the c10 olefins and the 1-olefins for species with fewer than 10 carbon atoms. The decenes are shown in Figure 22, together with the concentration of the n-decane fuel.

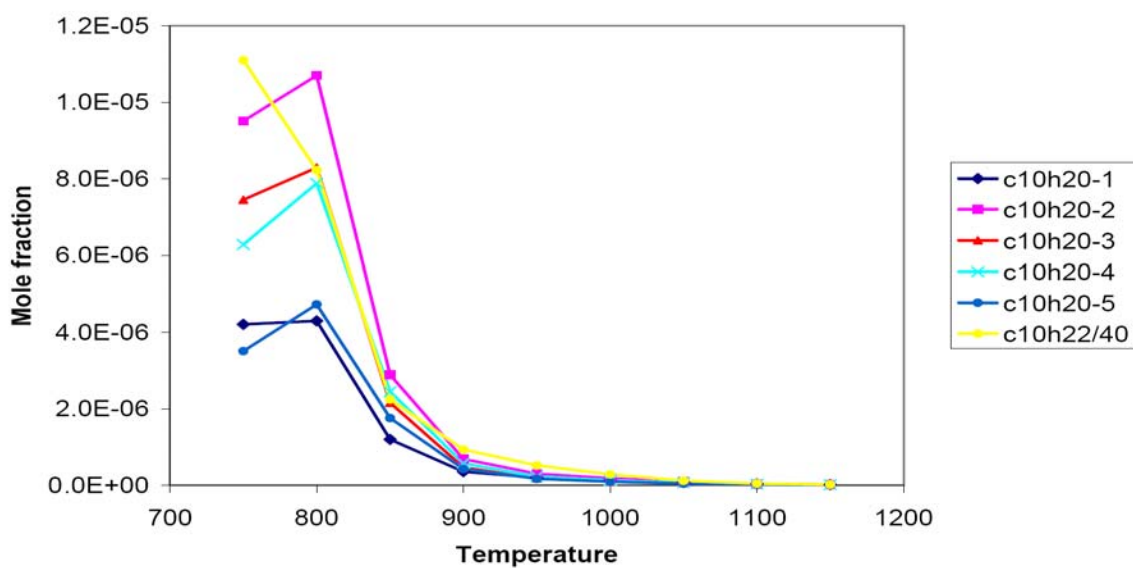


Figure 22. Computed levels of decenes produced in oxidation of n-decane in jet-stirred reactor. Concentration of n-decane is shown for comparison.

The decenes have their highest concentrations at relatively low temperatures, where the fuel consumption rate is greatest. Production of conjugate olefins during n-alkane oxidation is relatively difficult because it requires breaking a C-H bond following H atom abstraction from the fuel, rather than breaking a C-C bond via β -scission or addition of molecular oxygen, both of which are faster at temperatures around 800K. The 1-decene is produced at low rates because it requires breaking a primary C-H bond with its higher bond energy than secondary C-H bonds. The 5-olefin also is produced at low levels because it has only one reaction sequence for production, in contrast to the multiple formation pathways for the 2-, 3-, and 4-decenes.

In contrast, for all of the olefins with fewer than 10 carbon atoms, the present mechanism predicts that the 1-olefins have much higher concentrations than the other olefins with the same number of carbon atoms. Thus, for example, 1-octene is much more abundant than 2-octene, 3-octene or 4-octene in the n-decane simulations. This trend is easy to explain as a result of β -scission of alkyl radicals produced from H atom abstraction from n-decane, and the pattern is observed for combustion of all of the n-alkanes in both kinetic modeling and experiments.

The relative concentrations of 1-olefins produced from n-decane are shown in Figure 23, showing that those olefins with multiple production reaction pathways have much higher concentrations than those with more limited production pathways with higher energy barriers. Note that the c9 1-olefin, like the 1-decene discussed above, has a very low

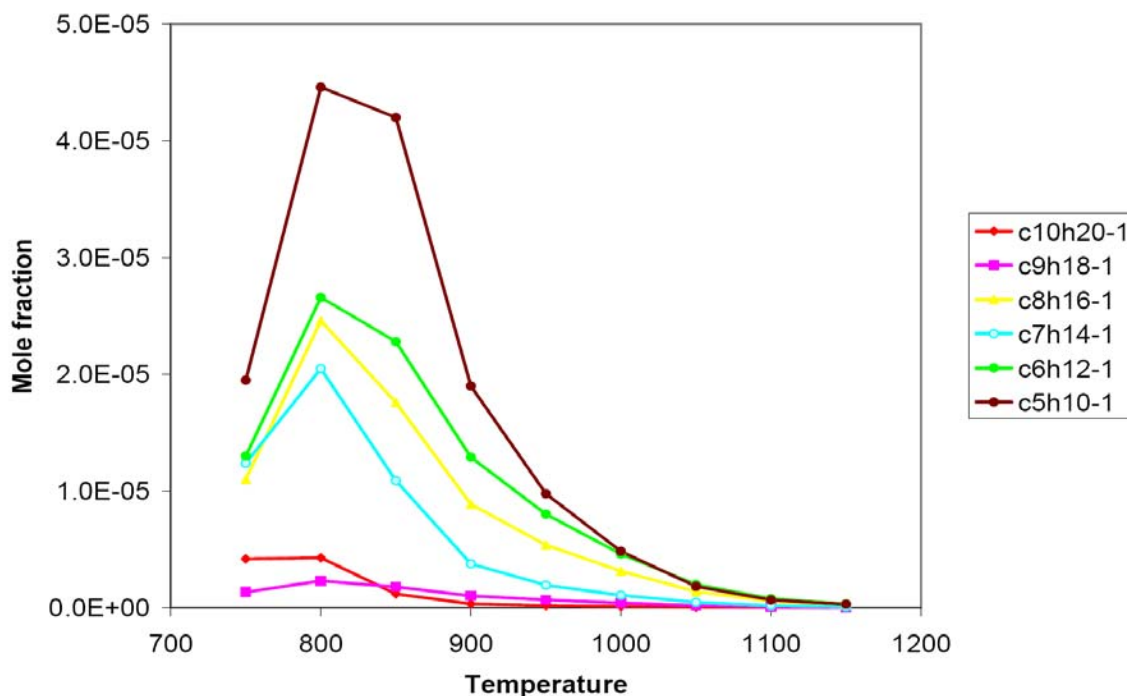


Figure 23. Concentrations of 1-olefins produced during oxidation of n-decane in a jet-stirred reactor.

concentration, which is due to its unique production path which requires abstraction of an H atom from the 3-site in n-decane followed by breaking the C-C bond between the first and second carbon atoms in the linear chain.

In a series of jet-stirred reactor experiments, with accompanying high temperature kinetic modeling, Dagaut et al. [34] reported results from an interesting family of n-decane/O₂/N₂ mixtures, with very dilute inlet fuel concentrations (700 ppm n-decane) over a wide range of oxygen concentrations from lean to very rich.

Jet stirred n-hexadecane results

Experimental and computed results were reported for stirred reactor oxidation of n-hexadecane by Ristori et al. [30], and additional kinetic analysis and modeling of the same experiments were reported by Fournet et al. [29]. The present kinetic mechanism for n-hexadecane provides very comparable level of agreement between computed and experimental species profiles in each of these experiments, similar to the results for n-decane.

We then used the kinetic mechanisms for all of the n-alkanes to carry out a series of numerical experiments under the same jet-stirred reactor conditions as those reported above for n-decane by Dagaut et al. [34]. We repeated the stoichiometric experiments for 700 ppm n-decane, with residence time of 0.07 seconds at atmospheric pressure for n-octane, n-dodecane and n-hexadecane. We scaled the inlet concentrations for each n-alkane to match the carbon atom flux with that for n-decane; therefore the inlet levels were (n-octane/O₂) = (875 ppm/10938 ppm), for n-cetane (700 ppm/10850 ppm), for n-dodecane (583 ppm/10750 ppm), for n-tetradecane (500 ppm/10750 ppm), and for n-hexadecane (438 ppm/10718 ppm). This approximately also scales the total H atom flux, although the H atom amounts decrease slightly as the carbon content remains constant.

The results of the jet-stirred reactor calculations are shown in Figure 24, showing the fuel concentrations for n-octane, n-decane and n-dodecane, under conditions of constant C atom input flux.

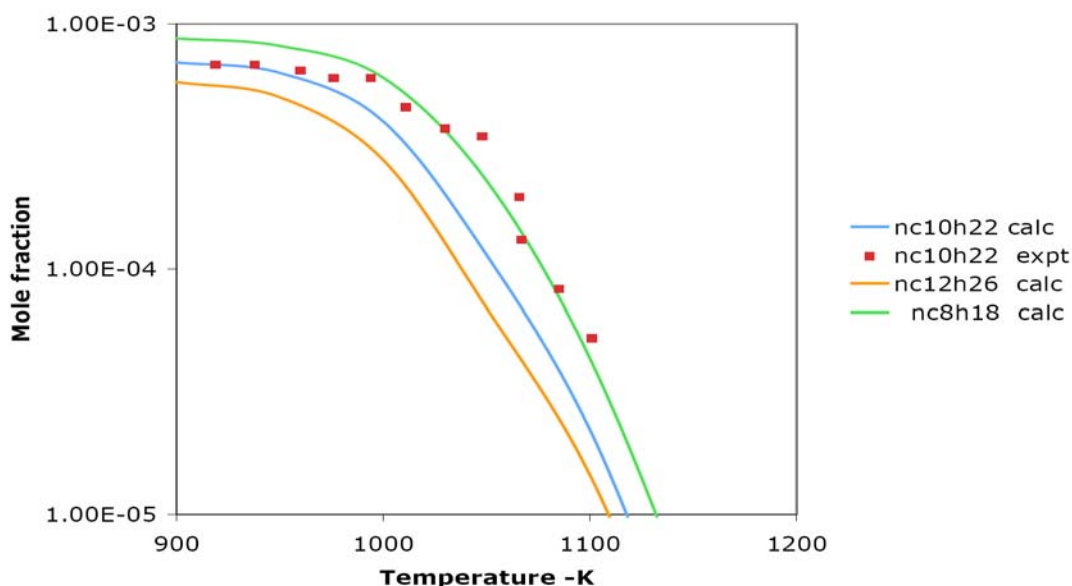


Fig. 24. Fuel concentrations in jet-stirred reactor simulations. Initial values are scaled to 700 ppm for n-decane for comparison. Experimental values are shown for n-decane (symbols) [34].

The fuel curves are displaced from each other in order to keep the carbon flux constant for all of the mixtures, but a much different result is observed for nearly all of the other species in the group of calculations, as shown in Figure 25 in which the levels of ethene, methane and 1-butene are plotted. The computed concentrations of these species, and most others not shown, are very nearly equal to each other, regardless of the n-alkane fuel being used. The similarities exist independently of the differences between the computed and experimentally measured values shown for n-decane fuel shown in Fig. 24. From these results, it appears that any large n-alkane fuel could serve as a reliable surrogate for any of the others. In this case, n-octane, n-dodecane, n-tetradecane and n-hexadecane all predict the same values for the major intermediates shown in Fig. 25 and for most other species as well. Accordingly, n-octane or n-decane would be very acceptable surrogates for a larger fuel such as n-hexadecane, thereby reducing significantly the computational costs of kinetic simulations. The only species not reliably simulated with this approach are the larger stable species associated with the larger fuel that are not included in the mechanism for the smaller surrogate fuel.

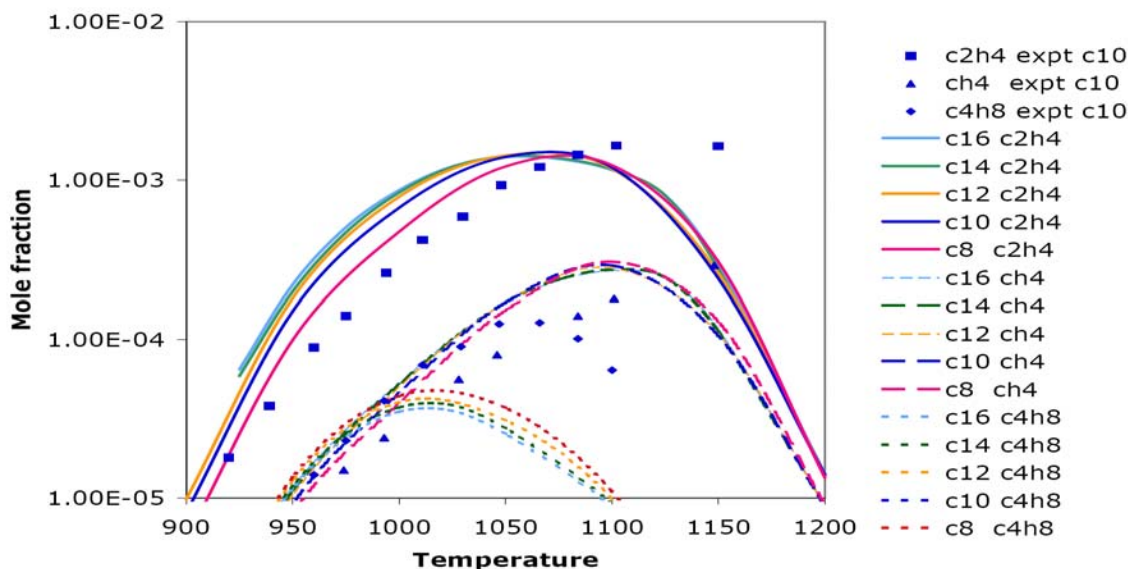


Fig. 25. Computed concentrations of ethene, methane and 1-butene for n-alkane fuels under jet-stirred reactor conditions. Symbols represent experimental values from Dagaut et al. [34] for n-decane oxidation.

Using Fig. 23 for illustration, concentrations of the n-decane fuel products 1-decene and 1-nonene are anomalously small due to their small production rates via limited reaction pathways that would not be limited if the fuel were n-dodecane or n-hexadecane. Therefore n-decane would be expected to predict levels of 1-octene and smaller 1-olefins but not for 1-decene or 1-nonene if it were used to simulate results for n-hexadecane or another larger n-alkane.

As noted by Dagaut and Cathonnet [49], these effects are sufficient to simulate overall reactivity, heat release and many intermediate species levels, but this approach is still

unable to address other questions such as sooting and the influences of aromatic species in the fuel. When the concern is aromatic species or soot production from an aliphatic fuel, reaction mechanisms with these features can be included with the n-alkane mechanism. Since the n-alkane mechanisms all predict very similar levels of unsaturated and other small hydrocarbons including acetylene and many others, aromatic species and soot formation for a large n-alkane such as n-hexadecane should be expected to be quite reliable if a mechanism for a much smaller n-alkane, with a suitable soot precursor kinetic mechanism, is used as a surrogate. When the fuel itself includes significant amounts of aromatic species, then use of a multicomponent surrogate which includes a relevant aromatic compound is required, as noted by Dagaut and Cathonnet.

High pressure flow reactor experiments

Agosta et al. [83] used a pressurized flow reactor to study autoignition and combustion of several components of a proposed surrogate jet fuel. One of the components was n-dodecane, and they used a semi-detailed kinetic model to analyze their measured results, showing reasonably good agreement. Related analysis of the same measurements was carried out in a larger study of semi-detailed kinetic mechanisms by Ranzi et al. [51]. We have used the same experimental data to test the present mechanism for n-dodecane.

The experiments on n-dodecane were carried out at 8 atm pressure for dilute lean mixtures. The inlet temperature of the reactants and nitrogen diluent was varied slowly from about 900K down to about 600K, and the overall reactivity was determined by measuring the CO concentrations in the reacting gases after an experimental residence time of 120 ms. The time constant for the inlet temperature variation is much longer than the reactant residence time in the flow reactor, so the reacting conditions are assumed locally time independent. No other species concentrations are measured in these experiments, so simulations of these results depend on the mechanism ability to predict CO levels for these n-alkane fuels. We noted earlier that predicted CO concentrations for the Princeton flow reactor experiments of Zhao et al. [42,43] for n-decane were not as accurate as for some other intermediates, but we expect that the relative CO concentration predictions should be more accurate than the absolute concentrations, and these experiments can still be valuable for mechanism validation.

We carried out detailed simulations of these pressurized flow reactor experiments, focusing on one case at an equivalence ratio of 0.2 and another case at $\phi = 0.3$, and the resulting CO results are compared with the experimental data in Figure 26.

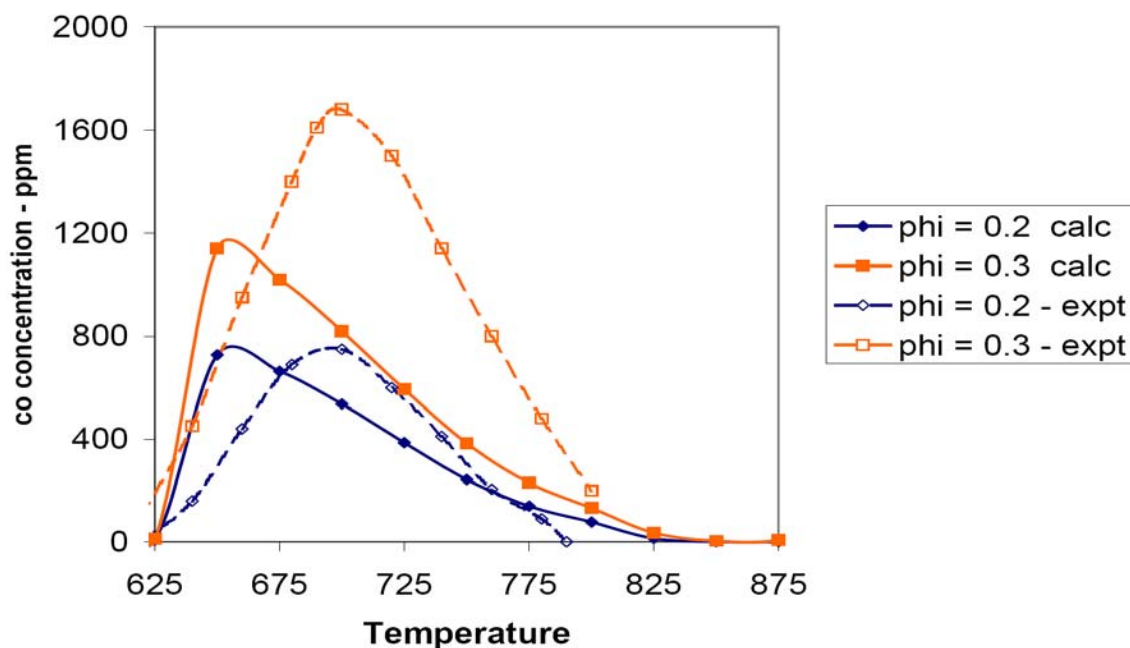


Fig. 26. Computed and experimental CO concentrations in pressurized flow reactor [83]

All n-alkane oxidation in the temperature range of these pressurized flow reactor experiments is strongly influenced by low temperature, alkylperoxy radical isomerization kinetics, and production of CO is close to the end of that reaction sequence. The degree of agreement between measured and computed values in Fig. 26 is a very demanding test of the validity of the kinetic mechanism. At both values of equivalence ratio, the kinetic model shows that the peak reaction zone is shifted slightly towards lower temperatures, compared to the measurements. The same type of shift toward lower temperatures was observed by Ranzi et al. using their semi-detailed or lumped kinetic model, although the shift was less in their simulations than that shown in Fig. 26. The good agreement in the absolute peak levels of CO also provides support for the reaction mechanism.

N-alkane thermolysis

Large n-alkanes are of considerable interest in various process engineering applications. As a result, there are many studies of conversion of n-alkanes to other chemical species as potential products, and one such study was selected for mechanism validation. In this study by Zhou et al. [84], n-alkane thermal pyrolysis, or thermolysis, of n-nonane, n-dodecane, n-tridecane, and n-hexadecane was studied at temperatures from 623K to 893K.

Under these conditions, 10% - 40% of the n-alkane fuel was consumed, leading primarily to 1-olefins from ethene up to the 1-olefin with the same number of carbon atoms as the n-alkane fuel. Overall, yields of 1-olefins decreased with increasing molecular weight; very little of the 1-olefin with the same number of carbon atoms as the fuel was produced, and the next-smaller 1-olefin production was also quite small. Note that these trends are very similar to those for 1-olefin production noted above in the jet-stirred reactor discussion in Figs. 22 and 23.

Computed results for product distributions are compared with the experimental results in Figure 27 for n-dodecane at atmospheric pressure and 893K. The overall agreement is quite good, and the kinetic model correctly identifies ethene as the major product, although the model overpredicts its absolute level. The highest concentration large 1-olefin is 1-c6h12 in both the model and the experiments, and although not shown in the figure, the levels of 1-undecene and 1-dodecene are very small in both the experiments and the calculations. The main difference between the experimental and computed results is that the experimental results were obtained after a residence time of 3.3 seconds, while the model predicted the same conversion of n-dodecane after only 1 second.

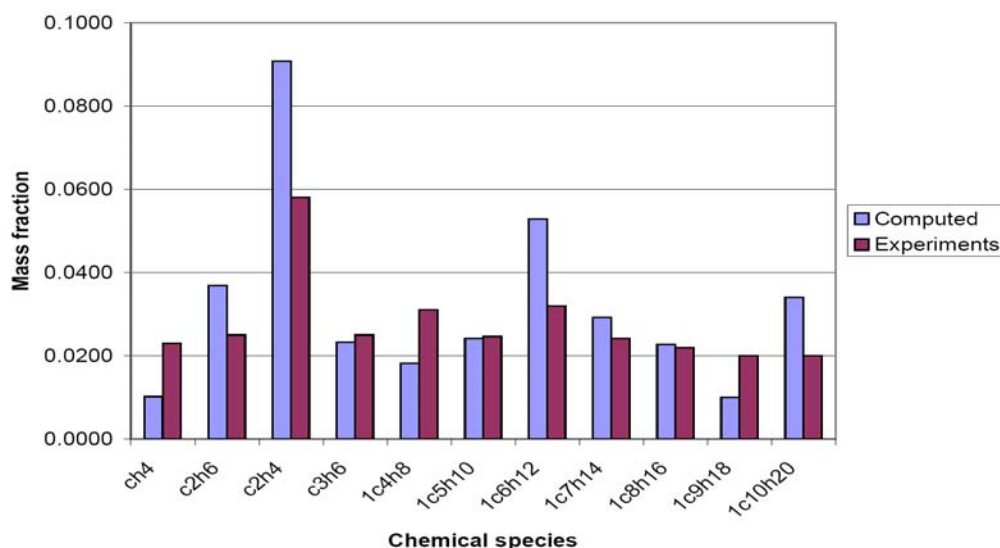


Figure 27. Products of n-dodecane thermolysis at 893K, experiments from Zhou et al. [84].

Similar agreement was observed for thermolysis of n-nonane, shown in Fig. 28. Again, most of the predicted product levels are quite close to the experimental results, while the ethene level is again overpredicted by the model. In the case of n-nonane, the time required for 9.3% conversion is 1.5 seconds where the product concentrations were measured as shown in Fig. ny, while the model produced the same n-nonane conversion in about 0.5 seconds. so the rates of conversion in the model appear to be approximately three times greater than in the experiments, although the product distributions are very similar between the model and the experiments.

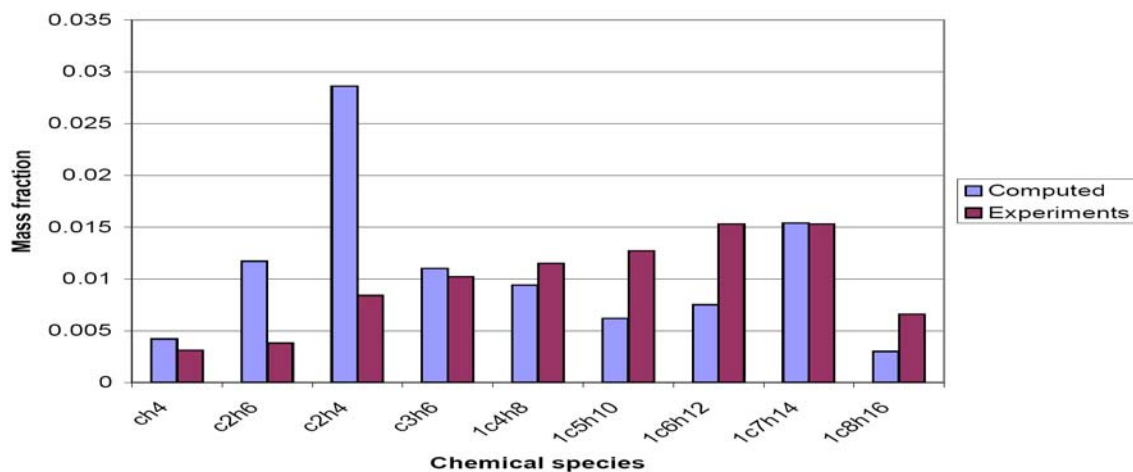


Fig. 28. Products of n-nonane thermolysis at 893K, experiments from Zhou et al. [84].

Pyrolysis of n-dodecane

Herbinet et al. [45] carried out a series of gas-phase pyrolysis experiments, using 2% n-dodecane in 98% He diluent, in a jet-stirred reactor specially designed to study thermal decomposition of liquid hydrocarbons. Experiments were carried out at temperatures from 773K to 1073K, and concentrations of 32 chemical species produced during the pyrolysis were measured at residence times from 1 to 5 seconds, including hydrogen, small saturated and unsaturated hydrocarbons, a wide range of 1-alkenes, and a variety of small aromatic, polyaromatic and cycloparaffin species. Herbinet et al. also carried out modeling simulations of their experimental results, using a mechanism for combustion of n-dodecane produced from their EXGAS software [25-29], in which they included reaction pathways forming and consuming aromatic compounds. Aromatics are a relatively minor product of the pyrolysis, and in our validation simulations, we did not include the aromatic or the cycloparaffin species formation reactions in order to focus on the n-alkane portion of the pyrolysis process.

At a residence time of 1 second, pyrolysis is slow for temperatures below 800K, proceeds more rapidly at higher temperatures, dominated by production of 1-alkenes in the temperature range from about 875K to 975K, and 1-alkenes are consumed rapidly at temperatures above 1000K. All of these features are reproduced very well by the present reaction mechanism. The major products of these experiments were hydrogen, methane, ethene, and propene, followed by a series of 1-alkenes from ethene to 1-undecene, with smaller levels of aromatic and cyclic paraffins, and a sample of these results are shown in Figure 29. Percent conversion of n-dodecane and production of methane, ethene and propene all show excellent agreement between measured and computed values.

Most of the 1-alkenes larger than propene are somewhat overpredicted by the present mechanism, as seen from the 1-decene profile in Fig. 29, with very similar results for 1-hexene, 1-heptene, and 1-octene. However, the computed 1-undecene is slightly smaller than the experimental results, and the computed level of 1-nonene is also slightly smaller than the experimental values. It is possible that inclusion of formation reaction pathways for aromatics would reduce the 1-alkenes to levels closer to the experimental values, but we also investigated a reaction class not previously included in past mechanisms or the present models.

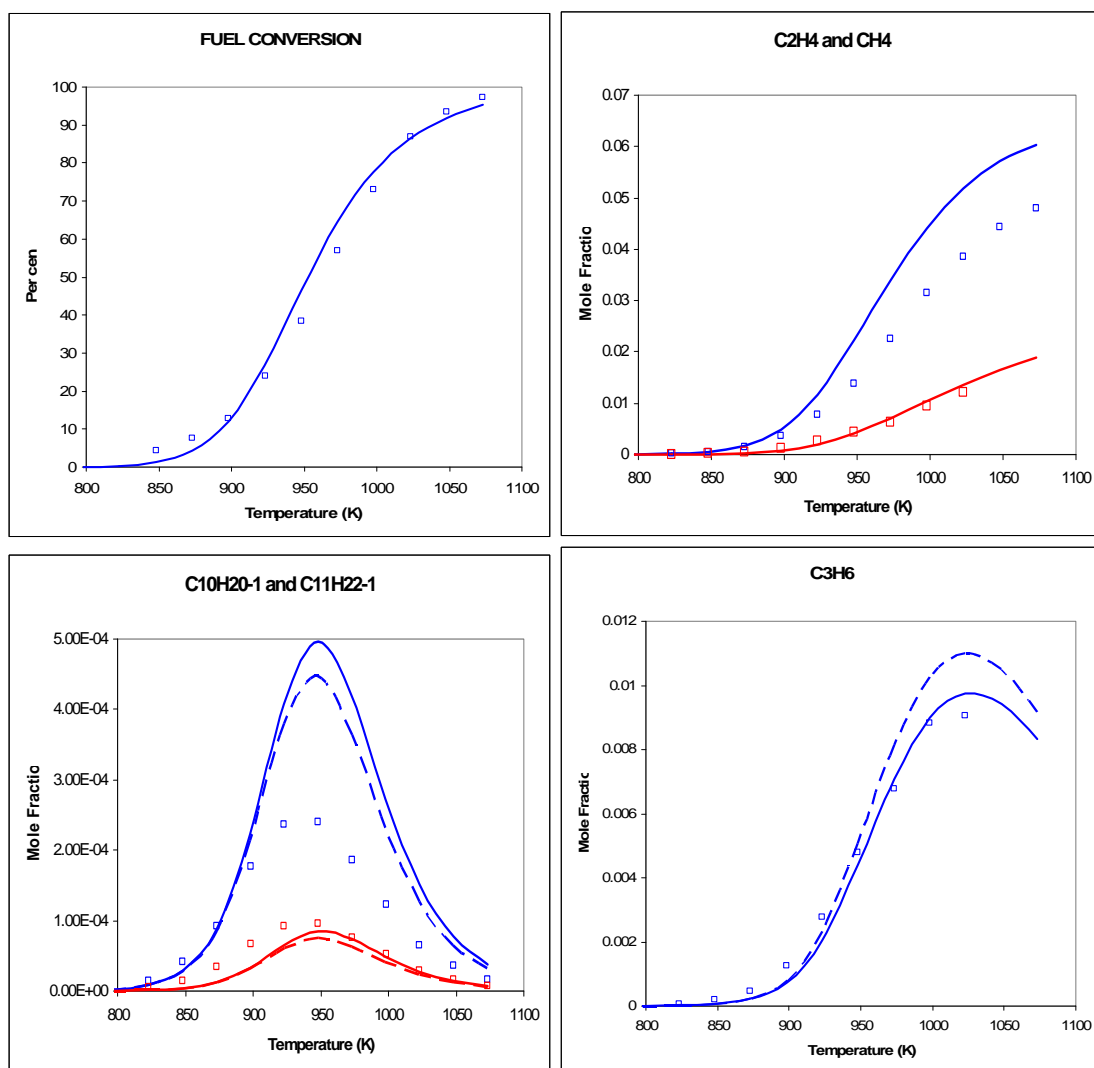


Fig. 29. Conversion of fuel and species produced in n-dodecane pyrolysis at 1 second residence time for a range of temperatures. Experimental values [45] are shown as symbols, lines show computed results, dashed curves include retroene reactions of 1-alkenes.

Retroene reactions of the 1-alkenes were introduced into the mechanism developed by Herbinet et al. [45,46]. These reactions represent a unimolecular decomposition pathway, involving a 1,5 hydrogen shift followed by a dissociation into a smaller 1-alkene and propene. The A factors and activation energies are smaller than those of the unimolecular decomposition of 1-alkenes via C-C bond scission [69], and they contribute to 1-alkene consumption only over the range of temperatures in this study.

Inclusion of these retroene reactions in the present n-alkane mechanisms produced only a relatively small change in the computed levels of the large 1-alkenes illustrated in Fig. 29. Propene levels are increased when retroene reactions are included, since each reaction produces additional propene, and the computed concentrations of the larger 1-alkenes are reduced, since the retroene reactions provide additional consumption pathways for these species. For the 1-alkenes that are overpredicted by the original mechanism, these reactions improve the agreement between computed and experimental results, and for 1-undecene and 1-nonene the agreement deteriorates. The influence of the retroene reactions of the 1-alkenes has little effect on the computed levels of the major product species, except for propene where the agreement is poorer when these reactions are included. They also have little effect on the rate of n-dodecane conversion.

Herbinet et al. also included concentration measurements over a range of residence times during pyrolysis of some selected mixtures and temperatures, which provides a somewhat different validation task than the measurements described above at a fixed residence time. In one such experiment, a mixture with 2% n-dodecane and 98% helium, at a temperature of 973K and at atmospheric pressure was studied, with a large variety of species concentrations measured at residence times from one to five seconds. We simulated this experiment with the present reaction mechanism, and the results are summarized in Figure 30.

These results show the evolution of the pyrolysis experiment, with the initial fuel decomposition converting the fuel into large 1-alkenes from 1-undecene to 1-hexene as intermediate products. The 1-alkenes are subsequently consumed, producing smaller 1-alkenes, eventually producing ethene, propene, methane and hydrogen. The time-dependent 1-alkene concentrations all have the same overall shape, with an initial increase to an elevated level, followed by consumption and conversion to final products.

These experiments were simulated as described above with two versions of the mechanism. In the first simulations, the 1-alkene retroene reactions described above were not included, and then they were added for a second set of simulations. These results are shown in Fig. 30, showing the major products ethene and methane, and two of the 1-alkene intermediates, 1-decene and 1-hexene. The regular mechanism overpredicts the intermediate levels of most of the 1-alkene intermediate species concentrations, although the computed profiles of the major products are quite accurate. When the retroene 1-alkene species decomposition reactions were included, the peak 1-alkene concentrations were reduced and became much closer to the measured values, as shown in Fig. 30.

These retroene reactions compete with abstraction reactions and C-C bond-breaking reactions of the 1-alkenes, both of which produce radical species, while the retroene reactions produce only olefinic products that are much less reactive. As a result, the inclusion of these reactions reduces the radical levels and slows the overall rate of reaction. A result of this slower rate of reaction is the reduced production rates of ethene, methane and 1,3-butadiene shown in Fig. 30.

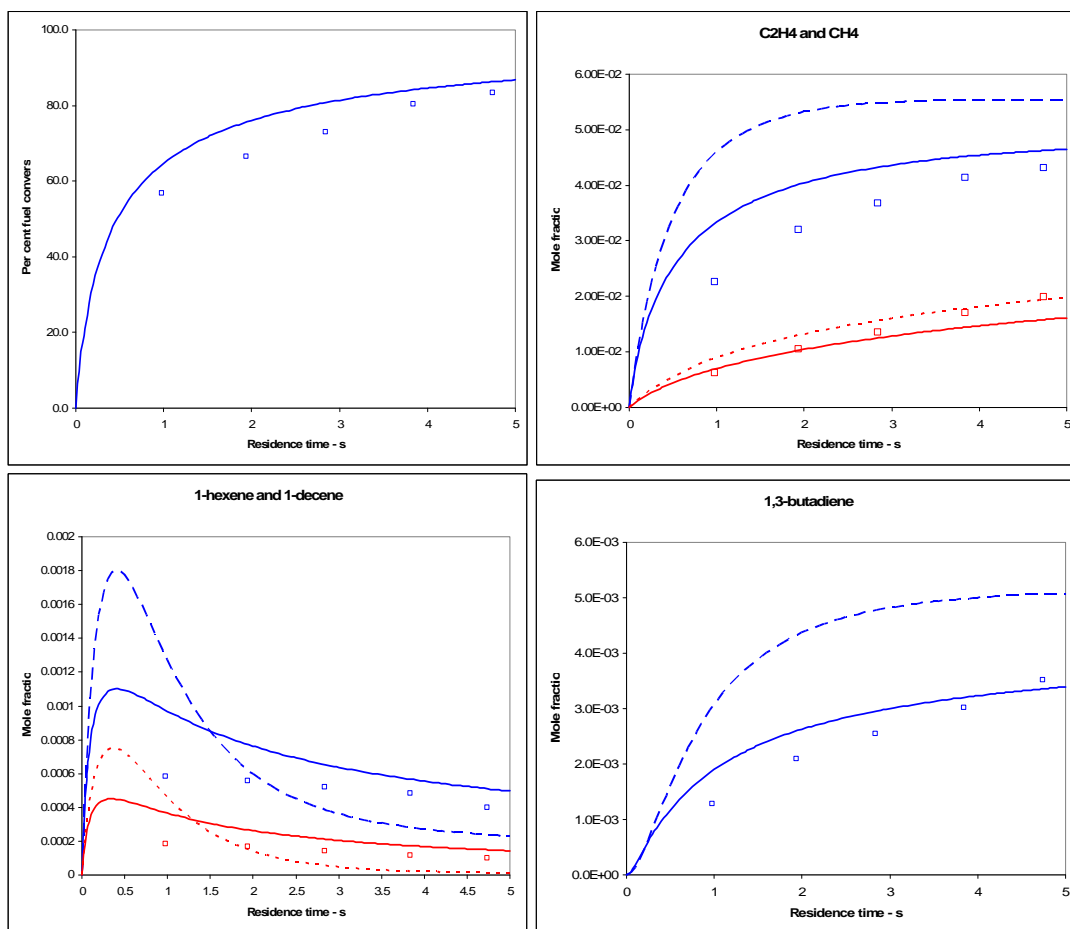


Fig. 30. Fuel conversion and species histories in n-dodecane pyrolysis [45]. Temperature is 973K, symbols are experimental points, lines are computed results. Solid curves include retroene 1-alkene decompositions, dashed curves do not include them.

The current reaction mechanisms do not include the retroene reactions of the 1-alkenes, but they will be included as part of future upgrades to the mechanisms.

SUMMARY

The kinetic mechanisms for the large n-alkanes described and tested here extend modeling capabilities that have been available for n-heptane for some years. Considerable attention has been given to providing the same level of kinetic detail that was contained in the previous n-heptane mechanism, so the experience that has been developed using the n-heptane mechanism should be directly applicable to these larger fuels.

The greater size of the new mechanisms make mechanism reduction an even more serious challenge than before, so these mechanisms should provide a valuable set of mechanisms to test reduction systems. The lumping techniques of Dryer [41-43] and Ranzi [22,48] have already been applied to mechanisms related to the present group.

These mechanisms also should be valuable in providing material for development of surrogate fuels [1-4] for practical systems as well as for unique systems such as biodiesel fuels. Large n-alkane species are prominent in transportation fuels, so the present mechanisms may be useful in making surrogate fuel mixtures more realistic than previously possible. A somewhat more subtle impact on surrogate fuel definitions has been provided by two of the n-alkane intercomparisons presented above that show that ignition and combustion of all of the n-alkanes from octane through hexadecane are remarkably similar. The ignition (see Fig. 6) and oxidation (see Fig. 25) of the n-alkanes, while not identical, are sufficiently close to each other that they can be exchanged for each other in many application simulations. This probably explains why our earlier n-heptane mechanism [9] has been so useful as a diesel fuel surrogate in past studies, despite its much smaller size than conventional diesel fuel molecules; its ignition rates are close enough to those of real diesel fuels, whose ignition rate and cetane number is established by its large n-alkane components, that diesel ignition is quite well reproduced by n-heptane.

Recent work of P. Dagaut et al. [31-35] has successfully used large n-alkanes as useful surrogates for kerosene and biodiesel fuels. The present work shows that the long straight-chain structure of the n-alkanes controls their ignition, and this clearly extends to long straight-chain molecules with additional functional groups attached to the end of the chain. The large n-alkanes should be successful as surrogates for other chemical species with similar structures, especially long-chain n-alkyl benzenes and n-alkyl cyclohexanes and cyclopentanes.

These mechanisms have been developed in somewhat simplified forms. We are already aware of numerous improvements that would make them more general and more applicable to new systems. Perhaps most important are extensions that would make them more specific towards kinetic modeling of olefins. Other refinements should provide a more accurate theoretical description of some kinetic processes, as well as more accurate extensions to much higher pressures. However, in the present form, these mechanisms have considerable capabilities for simulation of n-alkane fuels.

ACKNOWLEDGMENTS

This work was supported by the U.S. Department of Energy, Office of Freedom CAR and Vehicle Technologies, and the authors thank program managers Kevin Stork and Gurpreet Singh for their support of this work. This work was performed under the auspices of the U.S. Department of Energy by University of California, Lawrence Livermore National Laboratory under Contract W-7405-Eng-48.

REFERENCES

1. Pitz, W.J., Cernansky, N.P., Dryer, F.L., Egolfopoulos, F.N., Farrell, J.T., Friend, D.G., and Pitsch, H., "Development of an Experimental Database and Chemical Kinetic Models for Surrogate Gasoline Fuels", Society of Automotive Engineers paper SAE-2007-01-0175 (2007).
2. Farrell, J.T., Cernansky, N.P., Dryer, F.L., Friend, D.G., Hergart, C.A., Law, C.K., McDavid, R.M., Mueller, C.J., Patel, A.K., and Pitsch, H., "Development of an Experimental Database and Kinetic Models for Surrogate Diesel Fuels", Society of Automotive Engineers paper SAE-2007-01-0201 (2007).
3. Violi, A., Yan, S., Eddings, E.G., Sarofim, A., Granata, S., Faravelli, T., and Ranzi, E., "Experimental Formulation and Kinetic Model for JP-8 Surrogate Mixtures", *Combust. Sci. Technol.* 174, 399-417 (2002).
4. Colket, M., Edwards, T., Williams, S., Cernansky, N.P., Miller, D.L., Egolfopoulos, F., Lindstedt, P., Seshadri, K., Dryer, F.L., Law, C.K., Friend, D., Lenhert, D.B., Pitsch, H., Sarofim, A., Smooke, M., and Tsang, W., "Development of an Experimental Database and Kinetic Models for Surrogate Jet Fuels", AIAA publication (2007).
5. Lovell, W.G., "Knocking Characteristics of Hydrocarbons", *Ind. Engr. Chem.* 40, 2388-2438 (1948).
6. Westbrook, C.K., Pitz, W.J., and Leppard, W.R., "The Autoignition Chemistry of Paraffinic Fuels and Pro-Knock and Anti-Knock Additives: A Detailed Chemical Kinetic Study", Society of Automotive Engineers paper SAE-912314 (1991).
7. Westbrook, C.K., Pitz, W.J., Boercker, J.E., Curran, H.J., Griffiths, J.F., Mohamed, C., and Ribaucour, M., "Detailed Chemical Kinetic Reaction Mechanisms for Autoignition of Isomers of Heptane Under Rapid Compression", *Proc. Combust. Inst.* 29, 1311-1318 (2002).
8. Ribaucour, M., Minetti, R., Sochet, L.R., Curran, H.J., Pitz, W.J., and Westbrook, C.K., "Ignition of Isomers of Pentane: An Experimental and Kinetic Modeling Study", *Proc. Combust. Inst.* 28, 1671-1678 (2000).
9. Curran, H. J., Gaffuri, P., Pitz, W. J., and Westbrook, C. K., "A Comprehensive Modeling Study of n-Heptane Oxidation," *Combustion and Flame* 114, 149-177 (1998).
10. Curran, H.J., Gaffuri, P., Pitz, W.J. and Westbrook, C.K., "A Comprehensive Modeling Study of iso-Octane Oxidation", *Combustion and Flame* 129, 253-280 (2002).
11. Blurock, E.S., "Detailed Mechanism Generation. 1. Generalized Reaction Properties as Reaction Class Substructures", *J. Chem. Inf. Comp. Sci.* 44, 1336-1347 (2004).

12. Moreac, G., Blurock, E.S., and Mauss, F., "Automatic Generation of a Detailed Mechanism for the Oxidation of n-Decane", *Combust. Sci. Technol.* 178, 2025-2038 (2006).
13. Bikas, G., and Peters, N., "Kinetic Modelling of n-Decane Combustion and Autoignition", *Combust. Flame* 126, 1456-1475 (2001).
13. Westbrook, C.K., and Dryer, F.L., "Chemical Kinetics and Modeling of Combustion Processes", *Proc. Combust. Inst.* 18, 749-767 (1980).
14. Westbrook, C.K., and Dryer, F.L., "Chemical Kinetics Modeling of Hydrocarbon Combustion", *Prog. Energy Combust. Sci.* 10, 1- 57 (1984).
15. Westbrook, C.K., and Dryer, F.L., "A Comprehensive Mechanism for Methanol Oxidation", *Combust. Sci. Technol.* 20, 125-140 (1979).
16. Westbrook, C.K., and Pitz, W.J., "A Comprehensive Chemical Kinetic Reaction Mechanism for Oxidation and Pyrolysis of Propane and Propene", *Combust. Sci. Technol.* 37, 117-152 (1984).
17. Pitz, W.J., Westbrook, C.K., Proscia, W.M., and Dryer, F.L., "A Comprehensive Chemical Kinetic Reaction Mechanism for the Oxidation of n-Butane", *Proc. Combust. Inst.* 20, 831-843 (1984).
18. Li, J., Zhao, Z.W., Kazakov, A., Chaos, M., Dryer, F.L., and Scire, J.J., "A Comprehensive Kinetic Mechanism for CO, CH₂O and CH₃OH Combustion", *Int. J. Chem. Kinet.* 39, 109-136 (2007).
19. Li, J., Zhao, Z.W., Kazakov, A., and Dryer, F.L., "An Updated Comprehensive Kinetic Model of Hydrogen Combustion", *Int. J. Chem. Kinet.* 36, 566-575 (2004).
20. Held, T.J., and Dryer, F.L., "A Comprehensive Mechanism for Methanol Oxidation", *Int. J. Chem. Kinet.* 30, 805-830 (1998).
21. Hochgreb, S., and Dryer, F.L., "A Comprehensive Study on CH₂O Oxidation Kinetics", *Combust. Flame* 91, 257-284 (1992).
22. Ranzi, E., Sogaro, A., Gaffuri, P. Pennati, G., Westbrook, C.K., and Pitz, W.J., "A New Comprehensive Reaction Mechanism for Combustion of Hydrocarbon Fuels", *Combust. Flame* 99, 201-211 (1994).
23. Chevalier, C., Pitz, W.J., Warnatz, J., Westbrook, C.K., and Melenk, H., "Hydrocarbon Ignition: Automatic Generation of Reaction Mechanisms and Applications to Modeling of Engine Knock", *Proc. Combust. Inst.* 24, 93-101 (1992).

24. Battin-Leclerc, F., Fournet, R., Glaude, P.A., Judenherc, B., Warth, V., Come, G.M., and Scacchi, G., "Modeling of the Gas-Phase Oxidation of n-Decane from 550 to 1600K", *Proc. Combust. Inst.* 28, 1597-1605 (2000).
25. Warth, V., Stef, N., Glaude, P.A., Battin-Leclerc, F., Scacchi, G., and Come, G.M., "Computer-Aided Derivation of Gas-Phase Oxidation Mechanisms: Application to the Modeling of the Oxidation of n-butane", *Combust. Flame* 114, 81-102 (1998).
26. Warth, V., Battin-Leclerc, F., Fournet, R., Glaude, P.A., Come, G.M., and Scacchi, G., "Computer Based Generation of Reaction Mechanisms for Gas-Phase Oxidation", *Comput. Chem.* 24, 541-560 (2000).
27. Glaude, P.A., Warth, V., Fournet, R., Battin-Leclerc, F., Schacchi, G. and Come, G.M., "Modeling of the Oxidation of n-Octane and n-Decane Using an Automatic Generation of Mechanisms", *Int. J. Chem. Kinet.* 30, 949-959 (1998).
28. Fournet, R., Battin-Leclerc, F., Glaude, P.A., Judenherc, B., Warth, V., Come, G.M., Scacchi, G., Ristori, A., Pengloan, G., Dagaut, P., and Cathonnet, M., "The Gas-Phase Oxidation of n-Hexadecane", *Int. J. Chem. Kinet.* 33, 574-586 (2001).
29. Ristori, A., Dagaut, P., and Cathonnet, M., "The Oxidation of n-Hexadecane: Experimental and Detailed Kinetic Modeling", *Combust. Flame* 125, 1128-1137 (2001).
30. Bales-Gueret, C., Cathonnet, M., Boettner, J.-C., and Gaillard, F., "Experimental Study and Kinetic Modeling of Higher Hydrocarbons Oxidation in a Jet-Stirred Flow Reactor", *Energy and Fuels* 6, 189-194 (1992).
31. Dagaut, P., Reuillon, M., Boettner, J.-C., and Cathonnet, M., "Kerosene Combustion at Pressures up to 40 Atm: Experimental Study and Detailed Chemical Kinetic Modeling", *Proc. Combust. Inst.* 25, 919-926 (1994).
32. Dagaut, P., "On the kinetics of hydrocarbon oxidation from natural gas to kerosene and diesel fuel", *Phys. Chem. Chem. Phys.* 4, 2079-2094 (2002).
33. Dagaut, P., El Bakali, A., and Ristori, A., "The combustion of kerosene: Experimental results and kinetic modelling using 1- to 3-component surrogate model fuels", *Fuel* 85, 944-956 (2006).
34. Dagaut, P., and Gail, S., "Chemical Kinetic Study of the Effect of a Biofuel Additive on Jet-A1 Combustion", *J. Phys. Chem. A* 111, 3992-4000 (2007).
35. Dagaut, P., Gail, S., and Sahasrabudhe, M., "Rapeseed oil methyl ester oxidation over extended ranges of pressure, temperature, and equivalence ratio: Experimental and modeling kinetic study", *Proc. Combust. Inst.* 31, 2955-2961 (2007).

36. Dagaut, P., Reuillon, M., and Cathonnet, M., "High Pressure Oxidation of Liquid Fuels from Low to High Temperature. 3. n-Decane", *Combust. Sci. Technol.* 103, 349-359 (1994).
37. Bounaceur, R., Glaude, P.A., Fournet, R., Battin-Leclerc, F., Jay, S., and Pires da Cruz, A., "Kinetic modelling of a surrogate diesel fuel applied to 3D auto-ignition in HCCI engines", *Int. J. Vehicle Design* 44, 124-142 (2007).
38. Nehse, M., Warnatz, J., and Chevalier, C., "Kinetic Modeling of the Oxidation of Large Aliphatic Hydrocarbons", *Proc. Combust. Inst.* 26, 773-780 (1996).
39. Olchanski, E., and Burcat, A., "Decane Oxidation in a Shock Tube", *Int. J. Chemical Kinet.* 38, 703-713 (2006).
13. Bikas, G., and Peters, N., "Kinetic Modelling of n-Decane Combustion and Autoignition", *Combust. Flame* 126, 1456-1475 (2001).
41. Zhao, Z., Li, J., Kazakov, A., and Dryer, F.L., "Burning Velocities and a High-Temperature Skeletal Kinetic Model for n-Decane", *Combust. Sci. Technol.* 177, 89-106 (2005).
42. Zeppieri, S.P., Klotz, S.D., and Dryer, F.L., "Modeling Concepts for Larger Carbon Number Alkanes: A Partially Reduced Skeletal Mechanism for n-Decane Oxidation and Pyrolysis", *Proc. Combust. Inst.* 28, 1587-1595 (2000).
43. Held, T.J., Marchese, A.J., and Dryer, "A Semi-Empirical Reaction Mechanism for n-Heptane Oxidation and Pyrolysis", *Combust. Sci. Technol.* 123, 107-146 (1997).
44. Herbinet, O., Marquaire, P.-M., Battin-Leclerc, F., and Fournet, R., "Thermal decomposition of n-dodecane: Experiments and kinetic modeling", *J. Anal. Appl. Pyrolysis* 78, 419-429 (2007).
45. Dahm, K.D., Virk, P.S., Bounaceur, R., Battin-Leclerc, F., Marquaire, P.M., Fournet, R., Daniau, E., and Bouchez, M., "Experimental and modelling investigation of the thermal decomposition of n-dodecane", *J. Anal. Appl. Pyrolysis* 71, 865-881 (2004).
- x1. Lindstedt, R.P., and Maurice, L.Q., "Detailed Kinetic Modelling of n-Heptane Combustion", *Combust. Sci. Technol.* 107, 317-353 (1995).
- x2. Lindstedt, R.P., and Maurice, L.Q., "Detailed Chemical-Kinetic Model for Aviation Fuels", *J. Prop. Power* 16, 187-195 (2000).
46. Dagaut, P., and Cathonnet, M., "The ignition, oxidation, and combustion of kerosene: A review of experimental and kinetic modeling", *Prog. Energy Combust. Sci.* 32, 48-92 (2006).

47. Buda, F., Bounaceur, R., Warth, V., Glaude, P.A., Fournet, R., and Battin-Leclerc, F., "Progress toward a unified detailed kinetic model for the autoignition of alkanes from C4 to C10 between 600 and 1200K", *Combust. Flame* **142**, 170-186 (2005).
48. Ranzi, E., Frassoldati, A., Granata, S., and Faravelli, T., "Wide-Range Kinetic Modeling Study of the Pyrolysis, Partial Oxidation, and Combustion of Heavy n-Alkanes", *Ind. Eng. Chem. Res.* **44**, 5170-5183 (2005).
49. Battin-Leclerc, F., "Detailed Chemical Kinetic Models for the Low Temperature Combustion of Hydrocarbons with Application to Gasoline and Diesel Fuel Surrogates", *Prog. Energy Combust. Sci.*, submitted for publication, 2007.
50. Cohen, N., and Westberg, K.R., "The Use of Transition-State Theory to Extrapolate Rate Coefficients for Reactions of O-Atoms with Alkanes", *Int. J. Chem. Kinet.* **18**, 99-140 (1986).
51. Cohen, N., "The Use of Transition-State Theory to Extrapolate Rate Coefficients for Reactions of H-Atoms with Alkanes", *Int. J. Chem. Kinet.* **23**, 683-700 (1991).
52. E.R. Ritter, J. W. Bozzelli, "THERM - Thermodynamic Property Estimation for Gas-Phase Radicals and Molecules", *Int. J. Chem. Kinet.* **23** (1991) 767-778.
53. Yu, J., Sumathi, R., and Green, W.H., "Accurate and Efficient Method for Predicting Thermochemistry of Polycyclic Aromatic Hydrocarbons Bond-Centered Group Additivity", *J. Amer. Chem. Soc.* **126**, 12685-12700 (2004).
54. Allara, D.L., and Shaw, R., "A Compilation of Kinetic Parameters for the Thermal Degradation of Normal Alkane Molecules", *J. Phys. Chem. Ref. Data* **9**, 523-559 (1980).
55. Sun, H., and Bozzelli, J.W., "Thermochemical and Kinetic Analysis on the Reactions of Neopentyl and Hydroxy-Neopentyl Radicals with Oxygen: Part I. OH and Stable HC Product Formation", *J. Phys. Chem. A* **108** (10) (2004) 1694-1711.
56. Sheng, C.Y., Bozzelli, J.W., Dean, A.M., and Chang, A.Y., "Detailed Kinetics and Thermochemistry of $C_2H_5+O_2$: Reaction Kinetics of the Chemically-Activated and Stabilized CH_3CH_2OO Adduct", *J. Phys. Chem. A* **106** (2002) 7276-7293.
57. DeSain, J.D., Klippenstein, S.J., Miller, J.A., and Taatjes, C.A., "Measurements, Theory, and Modeling of OH Formation in Ethyl plus O_2 and Propyl plus O_2 Reactions", *J. Phys. Chem. A* **107** (2003) 4415-4427.
58. Carstensen, H., Naik, C.V., and Dean, A.M., "Detailed Modeling of the Reaction of $C_2H_5+O_2$ ", *J. Phys. Chem. A* **109**, 2264-2281 (2005).
58. E.J. Silke, W.J. Pitz, C.K. Westbrook, M. Ribaucour, "Detailed Chemical Kinetic Modeling of Cyclohexane Oxidation", *J. Phys. Chem. A* **111** (19) (2007) 3761-3775.

59. Pitz, W.J. Naik, C.V., Mhaolduin, T.N., Westbrook, C.K., Curran, H.J., Orme, J.P., and Simmie, J.M., "Modeling and Experimental Investigation of Methylcyclohexane Ignition in a Rapid Compression Machine", *Proc. Combust. Inst.* 31, 267-275 (2007).
60. Bozzelli, J., and Pitz, W.J., "The Reaction of Hydroperoxy-Propyl Radicals with Molecular Oxygen", *Proc. Combust. Inst.* 25, 783-791 (1994).
61. Bozzelli, J., and Ritter, E.R., *Chemical and Physical Processes in Combustion*, The Combustion Institute, Pittsburgh, 103:459 (1993).
62. Mehl, M., Pitz, W.J., "A Wide Range Kinetic Modeling Study of Oxidation and Combustion of the n-Hexene Isomers", manuscript in preparation, 2007.
63. Vanhove, G., Ribaucour, M., and Minetti, R., "On the influence of the position of the double bond on the low-temperature chemistry of hexenes", *Proc. Combust. Inst.* 30, 1065-1072 (2005).
64. Pollard, R.T., *Comprehensive Chemical Kinetics, Vol. 17*, (C.H. Bamford and C.F.H. Tipper, Eds.), Elsevier, New York, 1977, p. 249.
65. Tsang, W., and Hampson, R.F., "Chemical Kinetic Database for Combustion Chemistry. 1. Methane and Related Compounds", *J. Phys. Chem. Ref. Data* 15, 1087 - 1279 (1986).
66. Sahetchian, K.A., Rigny, R., De Maleissye, J.T., Batt, L., Anwar Khan, M., and Mathews, S., "The Pyrolysis of Organic Hydroperoxides (ROOH)", *Proc. Combust. Inst.* 24, 637-643 (1992).
71. Rienstra-Kiracofe, J.C., Allen, W.D., and Schaefer, H.F., "The C₂H₅ + O₂ Reaction Mechanism: High-Level ab initio Characterizations", *J. Phys. Chem. A* 104, 9823-9840 (2000).
68. Petersen, E.L., Kalitan, D.M., Simmons, S., Bourque, G., Curran, H.J., and Simmie, J.M., "Methane/Propane Oxidation at High Pressures: Experimental and Detailed Chemical Kinetic Modelling", *Proc. Combust. Inst.* 31, 447-454 (2007).
69. Davidson, D.F., Herbon, J.T., Horning, D.C., and Hanson, R.K., "OH Concentration Time Histories in n-Alkane Oxidation", *Int. J. Chem. Kinet.* 33, 775-783 (2001).
70. Horning, D.C., Davidson, D.F., and Hanson, R.K., "Study of the High-Temperature Autoignition of n-Alkane/O₂/Ar Mixtures", *J. Propulsion Power* 18, 363-371 (2002).
71. Zhukov, V.P., Sechenov, V.A., and Starikovskii, A.Y., "Autoignition of n-decane at high pressure", submitted for publication (2007).

72. Zhukov, V.P., Tsyganov, D.L., Sechenov, V.A., and Starikovskii, A.Y., "N-Decane Ignition at High Pressures", Proceedings of the European Combustion Meeting, Belgium, April 2005.
73. Ciezki, H.K., and Adomeit, G., "Shock-Tube Investigation of Self-Ignition of n-heptane-Air Mixtures Under Engine Relevant Conditions", *Combust. Flame* 93, 421-433 (1993).
74. Pfahl, U., Fieweger, K., and Adomeit, G., "Self-Ignition of Diesel-Relevant Hydrocarbon-Air Mixtures under Engine Conditions", *Proc. Combust. Inst.* 26, 781-789 (1996).
75. Kumar, K., Mittal, G., and Sung, C.J., "Autoignition of n-Decane under High Pressure Conditions", Paper D05, Fifth US Combustion Meeting, March 25-28, 2007.
76. Dec, J.E., "A Conceptual Model of DI Diesel Combustion Based on Laser-Sheet Imaging", Society of Automotive Engineers publication SAE-970873 (1997).
77. Petersen, E.L., Lamnaouer, M., de Vries, J., Curran, H., Simmie, J., Fikri, M., Schulz, C., and Bourque, G., "Discrepancies between shock-tube and rapid compression machine ignition at low temperatures and high pressures", Proceedings of International Symposium on Shock Waves, July, 2007.
78. Cox, A., Griffiths, J.F., Mohamed, C., Curran, H.J., Pitz, W.J., and Westbrook, C.K., "Extents of Alkane Combustion During Rapid Compression Leading to Single- and Two-Stage Ignition", *Proc. Combust. Inst.* 26, 2685-2692 (1996).
79. Agosta, A., Cernansky, N.P., Miller, D.L., Faravelli, T., and Ranzi, E., "Reference components of jet fuels: kinetic modeling and experimental results", *Exper. Therm. Fluid Sci.* 28, 701-708 (2004).
80. Zhou, P., Hollis, O.L., and Crynes, B.L., "Thermolysis of Higher Molecular Weight Straight-Chain Alkanes (C9 - C22)", *Ind. Eng. Chem. Res.* 26, 846-852 (1987).